Detection of Surface Cracks in Metals Using Microwave and Millimeter-Wave Nondestructive Testing Techniques—A Review

Mohamed A. Abou-Khousa[ID], *Senior Member, IEEE*, Mohammed Saif Ur Rahman[ID],
Kristen M. Donnell[ID], *Senior Member, IEEE*, and Mohammad Tayeb Al Qaseer[ID], *Senior Member, IEEE*

Abstract— Integrity assessment of metallic structures requires inspection tools capable of detecting and evaluating cracks reliably. To this end, many microwave and millimeter-wave nondestructive testing and evaluation (NDT&E) methods have been developed and applied successfully in the past. Detection of fatigue cracks with widths less than 5 μm using noncontact microwave-based inspection methods was demonstrated in the 1970s. Since their introduction, these methods have evolved considerably toward enhancing the detection sensitivity and resolution. Undertaking key application challenges has attracted considerable attention in the past three decades and led to the development of the near-field techniques for crack detection. To address a need that cannot be fulfilled by other NDT&E modalities, innovative noncontact microwave and millimeter-wave NDT&E methods were devised recently to detect cracks of arbitrary orientations under thick dielectric structures. While the reported methods share the same underlying physical principles, they vary considerably in terms of the devised probes/sensors and the application procedure. Consequently, their sensitivity and resolution as well as their limitations vary. This article reviews the various crack detection methods developed to-date and compares them in terms of common performance metrics. This comprehensive review is augmented with experimental comparisons and benchmarking aimed to benefit NDT&E practitioners and researchers alike.

Index Terms— Antenna, detection, imaging, metals, microwaves, millimeter waves, near field, nondestructive testing and evaluation (NDT&E), probe, resolution, resonators, sensitivity, surface cracks.

I. Introduction

METAL components are extensively used in many safety-critical structures in a wide range of industries. Metals are susceptible to subsurface and surface cracking due to a variety of reasons including in-service loading and environmental stresses as well as fabrication and manufacturing irregularities [1], [2], [3]. The occurrence and propagation of cracks have adverse impact on the structural integrity and performance of metal components. Therefore, reliable inspection of metallic structures throughout their life cycle is critical to avoid failures.

To prevent structural failure, it is imperative to reliably detect the presence of cracks during routine inspection and subsequently repair them before the complete fracture point is reached. The repair strategy is directly influenced by the geometrical parameters (or morphology) of the detected crack [4]. Furthermore, the geometrical parameters of a given crack in a component are considered vital to assess the life span of the component and its fitness for service (i.e., residual life assessment). Therefore, the inspection should not only reveal the existence of the crack (detection), but also provide quantitative information about its characteristics (e.g., its spatial extent, orientation, and tip location/size). The inspection tool should also allow for monitoring the crack after the repair intervention to determine the efficacy of the applied repair method in arresting further crack growth.

There are many nondestructive testing and evaluation (NDT&E) techniques developed to inspect metallic structures toward detecting and characterizing cracks. These include standard techniques such as visual inspection, dye penetrant, ultrasonic testing, eddy current, magnetic particle testing, and radiography [5], [6], [7] as well as nonstandard techniques such as microwave and millimeter-wave NDT&E methods [8], [9], [10], [11], [12], [13], [14].

Microwave and millimeter-wave NDT&E methods have advanced since their introduction in terms of sensitivity and resolution as well as utility [11], [14]. Today, there is a wide range of microwave and millimeter-wave crack detection and characterization methods. The majority of the reported methods are categorized in this article as far-field [15], [16], [17], [18], [19], [20], [21], [22], [23], [24], [25], near-field [26], [27], [28], [29], [30], [31], [32], [33], [34], [35], [36], [37], [38], [39], [40], [41], [42], [43], [44], [45], [46], [47], [48], [49], [50], [51], [52], [53], [54], [55], [56], [57], [58], [59], [60], [61], [62], [63], [64], [65], [66], and resonator techniques [67], [68], [69], [70], [71], [72], [73], [74], [75], [76], [77], [78], [79], [80], [81], [82], [83], [84], [85]. The resonator techniques were introduced in the 1970s and were shown to detect cracks as small as 2 μm wide and 25 μm

Mohamed A. Abou-Khousa and Mohammed Saif Ur Rahman are with the Electrical Engineering and Computer Science Department, Khalifa University of Science and Technology, Abu Dhabi, United Arab Emirates (e-mail: mohammed.aboukhousa@ku.ac.ae; mohammed.urrahman@ku.ac.ae).

Kristen M. Donnell is with the Department of Electrical and Computer Engineering, Missouri University of Science and Technology, Rolla, MO 65409 USA (e-mail: kristen.donnell@mst.edu).

Mohammad Tayeb Al Qaseer is with the Department of Electrical and Computer Engineering (ECpE), Iowa State University, Ames, IA 50011 USA (e-mail: alqaseer@iastate.edu).

deep while operating at 10 GHz [67], [68]. The development of the far-field methods was motivated by the success of the mode-conversion technique reported first in the late 1960s [15] and further enhanced thereafter [16], [17]. Major application leaps resulted from the introduction of the near-field methods in the 1990s [26], [33]. Emerging inspection and structural health monitoring techniques which utilize active microwave thermography (AMT) [86], [87], [88], [89], [90] and radio frequency identification (RFID) concepts [91], [92], [93], [94], [95], [96], [97], [98], [99] have also been developed and applied.

The ubiquity of the microwave and millimeter-wave inspection techniques for surface crack detection stems from the fact that they overcome some of the limitations associated with standard NDT&E modalities [12]. Detecting and characterizing surface cracks using microwave and millimeter-wave NDT&E methods have been the objective of many endeavors. The noticeable advancements in this domain were reviewed in [12] and more recently in [13]. Motivated by the wide range of developed methods and probes, including those which were introduced within the last few years, this article addresses the need for an updated and inclusive review of the main methods, their merits, and limitations. This article is aimed at overviewing the current state-of-the-art methods while emphasizing their overall operational envelop. Besides stating the reported capabilities of the various methods, the coverage in this article gives an additional insight on the suitability of the methods to fulfill the application requirements as well as the main parameters which affect their performance. Compared to the previous articles, this article offers balanced coverage of the various methods augmented with experimental benchmarking to highlight their relative performance. It also features clear statements of the crack detection problem and definitions of the performance metrics. The common principles which govern the application of the reviewed methods are also succinctly covered herein.

This article begins by stating the crack detection problem and the expectation from the NDT&E methods in Section II. The basics of crack detection using microwaves and millimeter waves are reviewed in Section III including the underlying physical principles shared by the reviewed methods. Specifically, the interaction between the crack and the electromagnetic (EM) fields used to interrogate the surface under examination is described in this section. Thereafter, various microwave and millimeter-wave detection and characterization methods are reviewed in Section IV. Emerging crack detection methods are overviewed in Section V. The reviewed methods are compared in Section VI. Finally, a summary of the main observations and an outline of the outstanding challenges are given in Section VII.

II. PROBLEM STATEMENT

A. Nature of the Crack in Metal

A crack is a defect or an anomaly manifested as material discontinuity which develops in metals while in-service or during manufacturing due to various reasons [1], [2], [3], [4], [5], [6]. The most common surface-breaking cracks are those induced due to mechanical and thermal fatigue as well as corrosion and lack of fusion in welded parts. Fig. 1(a) shows an example
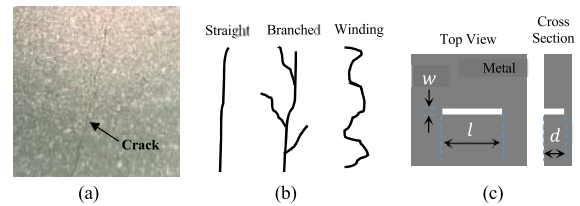

Fig. 1. (a) Photograph of a natural fatigue crack in steel. (b) Illustration of typical crack shapes. (c) Common crack model.

of mechanical fatigue crack in steel. Cracks can develop into different shapes including straight, winding, and branched [see Fig. 1(b)] [3], [6]. For instance, while mechanical fatigue cracks are generally straight, cracking due to corrosion has a high tendency to become branched [2], [3].

Surface cracks initiate on the metal surface and can grow under dielectric insulators of various thicknesses. Stress-induced corrosion cracks (SCCs) are typically filled with corrosion byproducts. Also, cracks can occur on curved surfaces such as joints and pipes. Fatigue cracks may also initiate around the fastener holes.

The geometrical parameters of a crack depend largely on the cracking mechanism, the stage of the crack (i.e., initiation versus propagation), and the material properties. During the crack initiation stage, the crack is typically "closed." As the propagation stage progresses, it can widen (open up) due to applied stresses. In this stage, the crack opening size (width) can range from a few to tens of micrometers. For example, previous investigations have shown that SCCs have openings between 16 and 32 μm and a tip radius of 1 μm or less [6].

It is quite common in the microwave and millimeter-wave NDT&E literature to use a simplified crack model consisting of a rectangular slot or notch of length, l, and width (opening), w, as shown in Fig. 1(c). The crack is assumed to have a uniform cross section that extends to a depth, d, through the thickness of the metal. This simplified model is commonly used in the theoretical analysis as well as for fabricating experimental crack samples (see [17], [26], [33]). However, some works have considered "V" and tilted crack models as well [45], [55]. Some of the recent literature has reported a crack model which consists of a cut with certain width and depth (see [52], [59], [60], [61], [62], [72], [74]). However, the representativeness of such a model when the length of the cut is a good portion of the wavelength was not thoroughly established, and qualification of the methods which adopted such a model on real crack samples was not reported in the literature.

B. NDT&E Requirements

Surface crack detection in practical inspection scenarios can be constrained by a multitude of factors acting individually or combined. The presence of the crack, its location, and geometry are unknown. Therefore, it is critical that the proposed NDT method allows for finding (discovering) the crack first (detection). This could be ideally accomplished using scanning-based techniques capable of rendering a distinguishable crack indication.

Another important ramification is that the orientation of the crack is oftentimes unknown as well. Hence, methods

which require "preferred" or known orientation(s) for reliable detection have limited applicability. Furthermore, the crack may be covered under a lossy dielectric such as corrosion, coating/paint, or relatively thick insulation. These dielectric layers may also be irregular surfaces (i.e., curved and/or possess a degree of surface roughness). Therefore, contact methods applicable for exposed cracks may not be well-suited for these cases. In addition, the sensitivity of noncontact methods to surface roughness should be minimized.

The main objective of the NDT method is to detect the crack with a high probability of detection in a practical environment (i.e., nonoptimum conditions). Quantitative characterization (evaluation) of the crack such as estimating its geometrical parameters (e.g., depth, length, opening/width, and orientation) becomes secondary to the detection problem. The application of the NDT&E method should be automated and ergonomic to reduce the potential for human error. It should also be reliable and robust against the environmental factors.

III. BASICS OF CRACK DETECTION USING MICROWAVES AND MILLIMETER WAVES

Commonly, microwaves and millimeter waves refer to EM waves of frequencies in the range from 300 MHz to 300 GHz. The wavelength, λ, corresponding to this frequency range spans from 1 m to 1 mm. A typical system which enables detecting a crack using these waves is described in Section III-A.

A. Top Level System Description

Fig. 2(a) shows a functional diagram of a basic micro/millimeter-wave crack detection system which is comprised of a probe/antenna, source/stimulus, detection subsystem, processing unit for acquisition, display, and control. The main components of this system are described next.

1) Antenna/Probe: Active microwave methods use a radiator (an antenna or probe) to stimulate/interrogate the surface under examination and detect the crack response. The probe/antenna is used to irradiate the structure with EM waves from a certain lift-off (or stand-off distance[1]) away from the surface of the metal. These EM waves induce a current density on the metal structure. The presence of a crack perturbs the current flow and alters the scattering/reflection characteristics of the metal. The same antenna/probe can be used to intercept the waves scattered from metal structure. The probe/antenna can be a single-port or two-port structure to enable the required measurements.

The perturbation caused by the presence of the crack is inferred by the resultant change induced in a specific measurement parameter (e.g., backscattered power, standing-wave voltage, magnitude/phase of the reflection coefficient, and shift in the resonant frequency). As detailed in Section IV, the majority of the crack detection works have been focused on the probe/antenna design.

2) Source and Detection Subsystems: Customized, relatively inexpensive, and battery-operated systems including

[1]While the term lift-off is used commonly in the general NDT literature, the term stand-off distance appears mainly in the microwave/millimeter-wave NDT literature.
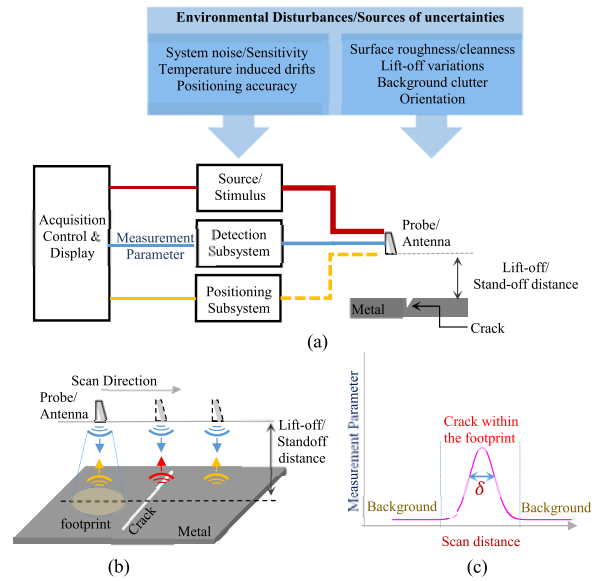

Fig. 2. (a) Functional diagram of typical microwave/millimeter-wave crack detection system. (b) Illustration of basic crack detection concept. (c) Example response.

reflectometers which employ standing-wave probes were used specifically with near-field crack detection methods [12]. In most of the recently reported research, vector network analyzers (VNAs) have been used extensively as stimulus/detection systems. VNAs are relatively expensive systems which employ tuned receivers and offer large dynamic range. They are capable of providing swept-frequency vector signal measurements represented as complex numbers. They are typically used to validate certain attribute of detection, and then, simpler systems designed to measure only the parameter of interest are used in practice. Most of the proposed crack detection methods operate at single frequency (i.e., continuous-wave systems). However, for some methods like wideband imaging methods which are overviewed later, a source capable of swept frequency measurements is needed.

3) Positioning Subsystem: In general, crack detection is performed by recording (or spatially indexing) the change in the measurement parameter relative to background. This may be accomplished using line scanning or imaging/mapping. The lift-off needs to be constantly maintained as most of the methods are sensitive to variations in this parameter. Most systems use raster scanning (C-scan) realized using 2-D positioning tables (sample moves under the probe) or Gantry type (the probe moves over the sample). Deployable flat/slightly curved and cylindrical scanners have been rarely reported with microwave and millimeter-wave systems designed for crack detection. For all types of positioning systems, the spatial sampling step size is very important to detect tight cracks.

B. Detection Concept

The fundamental concept behind microwave surface defect detection was eloquently articulated in [67] as "Suppose one is concerned with the detection of a surface defect on an otherwise smooth sample of a material. If, in some way, we illuminate this surface with microwaves, the defect will scatter some of the incident power: one can hope to detect this by looking for unusual reflected or transmitted signals."

This concept is illustrated with the aid of Fig. 2(b). When probe/antenna is scanned over the structure, the measurement parameter due to scattering when the crack passes through the footprint of the probe will be different than the parameter detected from the flawless background areas [see Fig. 2(c)]. The contrast/change in the measurement parameter gives direct indication of the presence of the crack. The crack indication represented as line scan is strong function of the footprint shape and size.

The behavior of the EM fields and their interaction with material structures are governed by Maxwell's equations and the set of boundary conditions prescribed for the geometry. There are a few basic physical observations which underpin the application of microwave and millimeter waves as stimuli in the crack detection problem [12].

1) These waves and their associated quantities such as the surface current density are sensitive to material discontinuities. A crack is essentially a discontinuity in the host metal. Therefore, its existence can be sensed indirectly through the perturbation it causes to the EM fields or associated quantities.

2) These waves propagate through air which enables remote interrogation and detection. Therefore, a noncontact inspection is possible based on these waves without the need for a coupling media (i.e., detection through air lift-off).

3) Beyond a very shallow skin depth, microwaves and millimeter waves do not penetrate inside good conductors. Hence, they are ideal for detecting surface cracks in conductors while being insensitive to the subsurface conductor features.

4) Microwaves and millimeter waves propagate through dielectric media which makes them appealing to interrogate cracks hidden under dielectric covers such as insulators, paint, rust, and dirt. Similarly, these waves can be used to detect cracks when filled with a dielectric material such as corrosion or dirt.

5) Microwaves and millimeter waves are sensitive to surface discontinuities in nonferromagnetic and ferromagnetic metals/alloys.

The development of microwave and millimeter-wave NDT&E techniques were motivated by the above listed observations [12]. When an EM wave radiation source such as the antenna/probe shown in Fig. 2 is used to irradiate the surface of the metal, it establishes a tangential electric field **E** and magnetic field **H** just above a metal surface. The linear current induced on the surface is given by [100]

$$\mathbf{J}_s \cong \hat{\mathbf{n}} \times \mathbf{H} \tag{1}$$

where $\hat{\mathbf{n}}$ is the unit vector normal to the surface. The tangential electric field is related to the linear surface current density by [100]

$$\mathbf{E} = Z_s \mathbf{J}_s \tag{2}$$

where Z_s is the surface impedance of the good conductor given by

$$Z_s = (1 + j)\sqrt{\frac{\omega\mu}{2\sigma}} \tag{3}$$
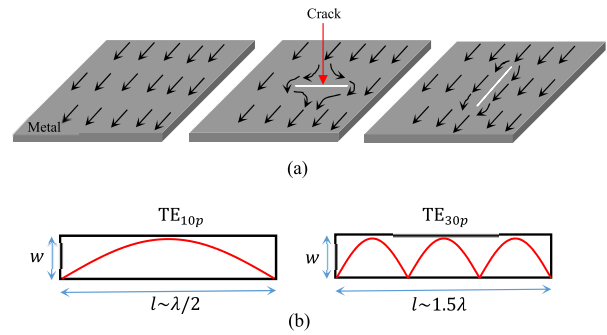

Fig. 3.   (a) Surface current (arrows) on a metal sample without and with a crack of two orthogonal orientations.[2] (b) Relative electric field distributions (magnitude) of the two TE modes on the crack's aperture.

and ω, μ, and σ are the angular frequency, permeability, and conductivity of the conductor, respectively.

As per (2), the surface current density and tangential electric field are related and they have the same general direction. As emphasized earlier, the presence of a crack in the surface is a discontinuity which perturbs the surface current flow [7], and consequently, the scattered electric field. The level or amount or perturbation of the crack causes is a function of the relative orientation between the crack and the surface current/tangential electric field as well as geometrical parameters of the crack. A crack maximally perturbs the current orthogonal to its length and minimally perturbs the current components which are parallel to its length as illustrated in Fig. 3(a) [16], [33]. In other words, the crack is a polarizing target.

An arbitrarily oriented crack results in a mode conversion, and this fact was devised in the early microwave crack detection methods [15], [16], [17]. Additionally, a portion of the currents can cross the crack surface in the form of displacement currents (i.e., across width of the crack). This displacement current is fundamentally related to the induced electric field on the crack opening. The induced electric field strength is maximum when the incident electric field vector is orthogonal to the crack's length [16]. In general, wider cracks (relative to the wavelength) cause stronger perturbation [33]. Therefore, the crack width also becomes an important parameter when detecting cracks using these techniques.

The response of the crack is a function of frequency. Based on the simplified crack model shown in Fig. 1(c), the crack behaves as shorted waveguide section [17], [33], cavity-backed slit, or simply a rectangular cavity. As such, the crack structure can support transverse electric (TE) and transverse magnetic (TM) modes (field distributions) [101]. In the microwave and millimeter-wave frequency ranges, the width of the crack, w, is very small compared to the wavelength. Furthermore, the width of a real crack is much less than its length ($w \ll l$). Therefore, the induced electric field in tight cracks at these frequencies does not vary over the width dimension, and the TM modes, if excited, will be evanescent modes (decaying exponentially away from the crack opening). The induced fields within the crack cavity which contribute significantly to its overall response can be expressed in terms of TE

---

[2]The surface current distribution is depicted in this simplified illustration to emphasize the main interaction mechanism. The displacement current over the crack opening is not shown here.

modes [17]. Specifically, the crack cavity can support TE_{m0p} modes where m and p are the integers corresponding to the number of half-cycle field variations over the length and depth dimensions, respectively. The zero in the mode designation TE_{m0p} reflects the fact that the field does not vary over the width dimension.

A resonant crack is generally regarded as one with length on the order of $\lambda/2$[3] or larger (resonance region) [17], [21], [66]. Such a crack is generally regarded as electrically large. The resonant frequencies of the TE modes depend on the size of cavity as well as dielectric that fills it. For example, Fig. 3(b) shows examples of the TE mode electric field distributions over the crack opening for two crack lengths (in terms of the wavelength). When the crack length is $\lambda/2$, one half-cycle is induced over the length (i.e., TE_{10p} mode). An additional half-cycle of variation appears for every $\lambda/2$ increase in the crack length. This is also illustrated in Fig. 3(b) for TE_{30p} mode where three half-cycles appear along the length of the crack.

Microwave and millimeter-wave signals can propagate inside electrically long cracks (in the resonance region). In this case, the response of the crack becomes a strong function of the depth [17]. A half-cycle field variation appears along the depth for each $\lambda/2$ section of length along that dimension. For instance, TE_{101} could be excited in a crack of length and depth of $\lambda/2$ (the crack is resonant along length and depth). This allows microwave and millimeter-wave NDT&E techniques to characterize the crack depth as well. This was utilized to determine the depth of cracks using far- and near-field techniques [17], [47]. Cracks much shorter than $\lambda/2$ cause weaker perturbation (Rayleigh region) [17].

The behavior of the crack in response to an incident wave can be generally explained using the above cavity model. Given the fact that the crack (cavity) response is maximum at resonance, the model allows for optimizing the frequency toward enhancing the detection sensitivity. This model is applicable to near-field and far-field applications. However, in the near-field methods, the evanescent TM modes can be significant and, therefore, cannot be neglected [33], [35].

C. Performance Metrics

In real application environments, the performance of microwave and millimeter-wave NDT&E systems is susceptible to various environmental disturbances and uncertainty sources as summarized in Fig. 2(a). Therefore, the system performance should be evaluated and optimized based on realistic application constrains in a given environment while taking into consideration the impact of the environmental disturbances. As articulated in [12], "The probes that were determined to be the optimal probes were indeed the probes, which produced a signal with a distinctive crack characteristic signal, had an adequately large dynamic range for the crack characteristic signal, were relatively unaffected by noise due to random surface roughness, were able to minimize lift-off issues through scanning repetition, and easily located the crack repeatedly." Therefore, it is not sufficient to establish the baseline performance while assuming "optimum conditions."

The key performance parameters to evaluate a given probe/system include the sensitivity and resolution. As per [102], the sensitivity is defined as the change in the measurement parameter over the change in crack parameter of interest. On the other hand, the resolution is defined in accordance with [102] as the smallest change in the crack parameter of interest which results in a distinguishable change in the measurement parameter. For surface cracks, the response due to a change in the crack width could be used to quantify the sensitivity and resolution, where "zero width" indicates no crack and is usually taken as the reference.

The sensitivity and resolution depend largely on the utilized probe, frequency of operation, and measurement parameter. The resolution allows for accurate determination of the crack's parameters. In assessing the sensitivity, the considered change in the crack parameter should be large compared to the resolution of the technique as stipulated in the sensitivity definition in [102]. Finally, the dynamic range corresponds to the span of the measurement parameter (output of the measurement system) resulting from the change in the crack parameter over certain relevant range.

The lateral resolution is another important metric used to quantify the performance of defect imaging/mapping techniques. The lateral resolution defines the shape of the response obtained after scanning/imaging a crack. In the example response illustrated in Fig. 2(c), the spatial resolution determines the width, δ, of the line scan response. Higher spatial resolution implies a smaller footprint, and consequently, a sharper indication of the detected crack.

The lateral resolution of the microwave/millimeter sensing methods which rely on interrogation using plane waves is fundamentally limited by the wavelength. This limitation has been realized early on and led to the introduction of open resonators with dimensions much less than the wavelength. As mentioned in [67], the simple concept is "to view the object through a small aperture in a metallic screen. The resolution which one can then attain is determined by the aperture diameter rather than by the wavelength of the illumination." Therefore, most of the resonator methods developed thus far devise small probes which can attain a lateral resolution better than the diffraction limit.

IV. DETECTION METHODS

Depending on the utilized detection method, the measurable manifestation of the perturbed current/field due to the crack differs.

A. Far-Field Methods

In the far-field methods, the cracked sample is located in the far-field of the used antenna.[4] In essence, the lift-off is larger than the far-field limit of the used antenna. The perturbed current initiates a scattered signal (reflection) which is different than the one established by un-perturbed current on the surface without a crack. Effectively, the scattered fields or energy (e.g., proportional to the radar cross section) from

---

[3]The wavelength inside the crack cavity (i.e., guide wavelength) as opposed to free-space wavelength.

[4]With a utilized antenna of largest dimension D operating at a wavelength λ, the crack will be in the antenna's far-field region if the lift-off is greater than $2D^2/\lambda$ [100].
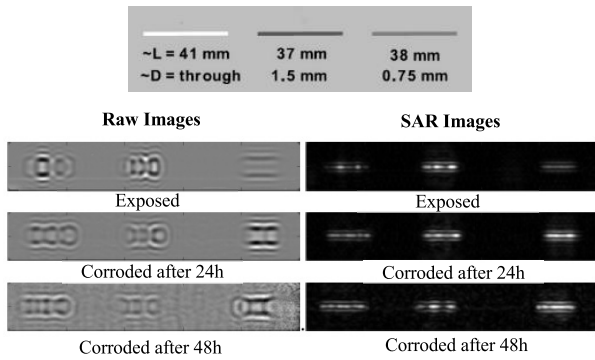
Fig. 4. Schematic (top) of a steel sample with various notches (*L*: length and *D*: depth), raw (at 38.65 GHz) and wideband SAR images of the exposed notches as well as when covered under corrosion developed after being in a salt-fog chamber for 24 and 48 h [19] (© 2017 IEEE).

Fig. 5. Photograph of the steel plate with corroded and uncorroded fatigue cracks (bottom) and their wideband SAR images (top) [19] (© 2017 IEEE).

the metal with and without a crack will be different. The approach follows classical radar measurements and can be conducted in mono- and bistatic configurations (reflection and transmission, respectively), in the frequency and time domains. When a crack is in the far field of an antenna, its presence does not change the current distribution on the antenna itself. The early mode conversion methods introduced in the 1960s and 1970s of the last century fall under this category [16], [17]. These methods demonstrated a capability to detect and characterize 50-μm-wide slots with depths ranging from $\sim$25 μm to 5 mm [16]. Also, the far-field methods include the recently proposed exposed/covered crack detection techniques based on synthetic aperture radar (SAR) imaging [18], [19], [20], [21], [22], [23], [24], [25].

The overall sensitivity of these methods is moderate because the radiator is far from the target. However, they are not sensitive to lift-off variation and can be applied over large distances. For instance, a Ka-band (26.5–40 GHz) SAR imaging system was recently used to detect and characterize cracks of various lengths and widths ranging from 0.25 to 0.875 mm at lift-off of 30 mm [21]. As demonstrated in [21], the sensitivity of these methods is a function of frequency (i.e., most sensitive when the crack is resonant at the operating frequency). They are ideally suited for sensing applications where the structure under examination cannot be brought close to the antenna and/or when the crack is covered under a thick insulator. The lateral imaging resolution depends on the size of the realized footprint, and it is bounded by the diffraction limit ($\lambda/2$ in the bistatic/transmission mode and $\lambda/4$ in the monostatic/reflection mode) [103].

With SAR imaging, cracks can be detected from large distances and through thick multilayered dielectric covers. However, to maintain the diffraction-limited resolution mentioned above, the scan domain size (area of synthetic aperture) must be about two times the lift-off or larger [103]. Understandably, the maximum lift-off will also be limited by the receiver sensitivity (the lowest detectable signal) and the gain of the antennas. However, using a higher gain antenna reduces the lateral resolution of the image [103].

Recently, SAR imaging methods were used to successfully detect cracks under severe corrosion conditions [19]. For instance, Fig. 4 shows the schematic of a metal sample with various notches along with their raw images (unfocused at single frequency) and wideband SAR images obtained using
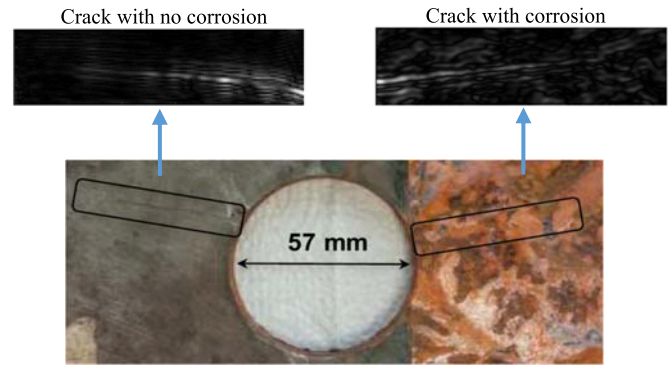
Ka-band rectangular waveguide (RWG) aperture at 9-mm lift-off for two cases of corrosion. The corrosion layers were developed by placing the metal sample inside a fog chamber for 24 and 48 h (to control the severity of the corrosion).

The notches shown in Fig. 4 are longer than the wavelength and would be electrically longer when the corrosion accumulates in them. The signature of the notches in the raw images clearly indicates the shape of the excited field modes with more cycles appearing over the length as the corrosion accumulates. The mode cycles are also evident in the SAR images. It is remarked here that the width of the crack indication in the SAR image does not correspond to the actual width of the notches. The width of the SAR-rendered notch indication is influenced by lateral resolution of the system. The method was also used to detect shorter and narrower notches as well as real stress-induced cracks, as shown in Fig. 5 [19].

Polarimetric SAR methods have also been applied recently to detect cracks of arbitrary orientations. Fig. 6(a) shows the setup of a recently reported polarimetric SAR method developed to detect cracks covered under thick insulation in the K-band frequency range (18–26.5 GHz) [24]. Fig. 6(b) shows one of the samples considered in [24] which consists of six 0.25-mm-wide electrical discharge machined (EDM) through notches covered under a 6.25-mm-thick Teflon insulator. Using this method, the cracks were detected reliably from 10 mm of lift-off with a dual-polarized circular aperture antenna [24]. The system reported in [24] enabled the construction of SAR images from the two co-polarizations and the cross-polarization measurements between the ports as reported in Fig. 6(c). The system was successfully used to detect cracks under a 12.7-mm-thick Teflon cover and a 4.3-mm-thick Rubber cover at a 10-mm lift-off from the surface of the cover [24]. The method can be improved in the future through the use of a four-port probe which enables two cross-polarized measurements (e.g., a pair of two orthogonal linear polarizations rotated in space by 45°.)

The main benefit of using the cross-polarization measurement is the ability to suppress the nonpolarized background (clutter) [16], [17], [22], [24] and thus, increasing the overall sensitivity of the system despite the large sensing distance and presence of the cover which may be lossy. This is evident in Fig. 6(c) by comparing the background noise in the co- and cross-polarized images. The method could be potentially used to detect cracks on slanted metal surfaces or when the cracks are covered by dielectrics with surface irregularities.
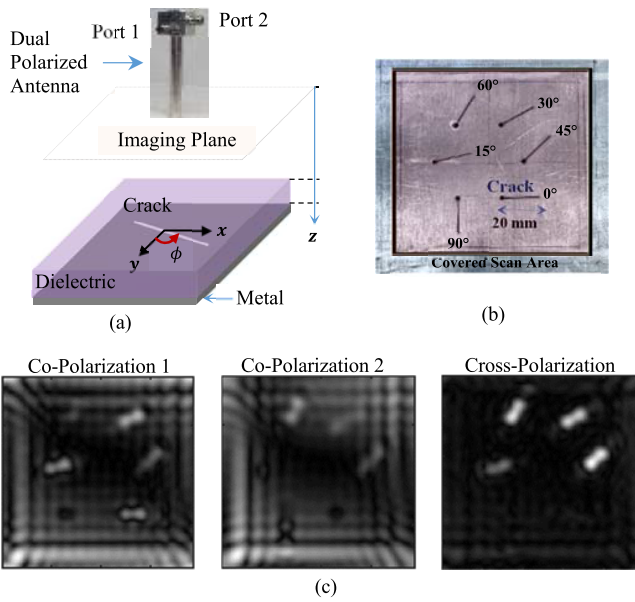
Fig. 6. (a) Covered crack detection setup with dual-polarized antenna. (b) Photograph of the EDM notches with various orientations. (c) Co- and cross-polarization SAR images [24] (© 2021 IEEE).
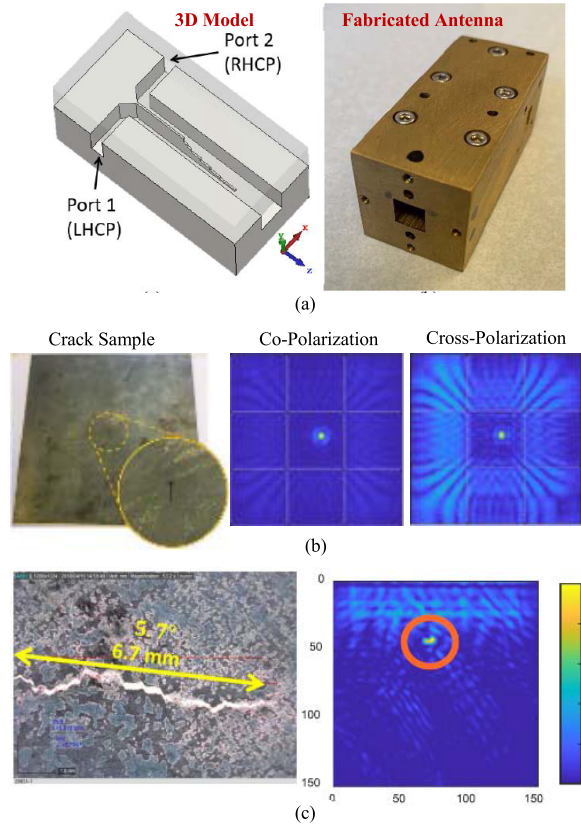

Fig. 7. (a) Model and photograph of the Ka-band dual circularly polarized antenna. (b) Photograph of the EDM notch and SAR images. (c) Photograph of the narrow crack and its SAR image [22] (© 2020 IEEE).

Using a dual orthogonal polarization also allows for estimating the crack orientation. In this case, the choice of polarization type is critical. Utilizing dual orthogonal linear polarizations will result in erroneous orientation estimation results when the crack becomes parallel to one of the polarizations. In such a case, the crack minimally scatters the parallel polarization which results in a loss of information in that polarization. On the other hand, using a circular polarization results in a scattering level that is independent of the orientation of the crack [22].

In [22], a dual circularly polarized Ka-band square aperture antenna excited with two ports to transmit and receive left- and right-hand circular polarization (LHCP and RHCP, respectively) was used for detecting cracks and estimating their orientation based on wideband SAR imaging. The proposed polarimetric SAR method in [22] allows for estimating the orientation of the crack from the phase difference between co- and cross-polarized scattering components. The model and photograph of the devised antenna are shown in Fig. 7(a).

The efficacy of using a dual circular polarization to detect short cracks from a large lift-off of 100 mm (10λ at 30 GHz) was demonstrated [22]. For instance, Fig. 7(b) shows a 4-mm-long and 0.5-mm-wide through-thickness EDM notch, and the corresponding co- and cross-polarization (left–left and left–right) wideband SAR images. Using wideband measurements, the maximum estimation error in the crack orientation was 4° for a 6-mm-long EDM notch imaged at a 50-mm lift-off. The system was also successfully used to detect real tight cracks and estimate their orientation. A photograph of the crack considered in [22] along with its estimated orientation angle and the co-polarized SAR image acquired at a lift-off of 100 mm are shown in Fig. 7(c). The capability of the method reported in [22] to suppress the reflection from the metal plate in the co-polarization channel depends on the axial ratio of the devised circularly polarized antenna.

Detecting and estimating the orientation of cracks using polarimetric SAR method with linearly polarized antennas rotating around a circle enclosing the crack sample was reported recently in [25]. While pointing at the center of the sample from an elevated plane, the antenna rotates, and consequently, the crack interacts with an incident field vector with various orientations. The method reported in [25] is based on intensity maximization through an iterative process. Using four Ku-band (12.4–18 GHz) horn antennas, the method was used to accurately estimate the orientation of a 2-mm-wide and 5-mm-long slit imaged at a 1-m lift-off with a maximum error of 5.1° and a root-mean-square error of 1.9°. A similar concept can be implemented in the future using a single antenna that radiates a radially polarized wave and detection using matched filters [104]. The performance of the SAR methods in [22] and [25] was established for exposed cracks. Future investigations can also consider covered crack scenarios.

B. Near-Field Methods

The near-field microwave and millimeter-wave techniques have shown great potential for various NDT&E applications [10]. The near-field probes developed in the past and demonstrated for crack detection include coaxial probes [26], [27], [28], [29], [30], [31], [32], RWG apertures [33], [34], [35], [36], [37], [38], [39], [40], [41], [42], [43], [44], [45], [46], [47], [48], [49], circular waveguide (CWG) apertures [53], [54], [63], and flanged parallel-plate waveguide [55]. An illustration of the RWG relative aperture sizes for various frequency bands is shown
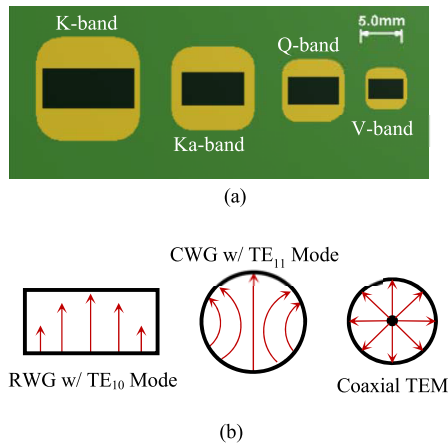
Fig. 8. (a) Cross section of various near-field RWG probes. (b) RWG (TE$_{10}$), CWG (TE$_{11}$), and coaxial line (TEM) electric field distributions.

TABLE I
LATERAL RESOLUTION OF SOME NEAR-FIELD APERTURE PROBES [77]

Probe	Size (mm)	Freq. (GHz)	Resolution (mm)
Loaded K-band Circular Aperture	6.25 Dia.	24	4
K-band Rectangular Aperture	10.7 × 4.3	24	5
Ka-band Rectangular Aperture	7.1 × 3.56	33	3.5
V-band Rectangular Aperture	3.76 × 1.87	70	1.8

in Fig. 8(a). These probes are typically excited with their dominant TE field mode (TE$_{10}$) [see Fig. 8(b)]. The CWG probes are commonly operated in their dominant TE$_{11}$ mode which is illustrated in Fig. 8(b). The coaxial probes support transverse electromagnetic (TEM) with radial field electric field components as shown in Fig. 8(b).

In the near-field methods, the source and/or detector of the EM radiation is tightly coupled to the crack. Effectively, they can be used in contact or with a lift-off which is smaller than the far-field limit of the probe. When the crack is in the near field of the probe, its presence changes the current distribution on the probe, and consequently, its near-field characteristics. One probe is typically used as both source and detector. In general, the presence of the crack manifests as a change in the complex reflection coefficient (scattering parameter S_{11}), measured at the input of the probe and referenced to the background.

Open-ended RWG probes have been the most prominent probes in the application of near-field techniques for crack detection and evaluation [12]. They can be used with dominant and higher order mode approaches [33], [34], [35]. They have demonstrated practical utility in detecting and characterizing exposed, covered, and filled cracks [12]. These simple near-field probes were extensively studied over the past three decades. They can be used with a simple battery-operated system, whereby the crack is detected based on observing the characteristic signal acquired using a standing-wave reflectometer when the probe is scanned over the crack [33]. The crack characteristic signal depends on the geometrical parameters of the crack, the probe aperture size, frequency of operation, and the location at which the standing wave is measured [41]. Using this approach, K- and Ka-band opened-ended waveguides operating at 24 and 33 GHz, respectively, were devised to characterize fatigue cracks of widths ranging from 3 to 50 μm [42].

Alternatively, the crack can be detected by observing the change in the complex reflection coefficient (S_{11}) measured at the input of the near-field waveguide probe. At zero lift-off, the waveguide is in contact with metal surface (short circuit) and the presence of the crack, once passed through the aperture area, is sensed through the change in the phase of the reflection coefficient [33], [47]. Assuming no losses, the

magnitude of the reflection coefficient remains unity in this case [47]. However, at nonzero lift-off and/or when losses are considered, the magnitude and phase both change due to the presence of the crack [47]. Using a noncontact approach, the inspection performance using these Ka-band probe operating at 33.5 GHz has been performed favorably compared to an industrial phased array ultrasonic testing (PAUT) system [51].

The sensitivity of the reflection-type near-field methods can be quantified in terms of the measured change in complex reflection coefficient (phase or magnitude) for a given crack geometry (e.g., width/depth). Similar to the far-field methods, the sensitivity of these methods is also a function of frequency. However, their sensitivity is relatively higher than the far-field methods and drops at large lift-offs. In addition, they are sensitive to lift-off variation. To address this challenge, lift-off compensation techniques can be applied (see [64], [65], and the references therein). The differential probe concept introduced in [63] was used to develop a W-band (75–110 GHz) probe which enabled the detection of cracks near fasteners and under paint in an aircraft fuselage [66]. In this near-field application, the resonant behavior of the crack was leveraged to realize a sensitive method in a complex inspection environment [66]. In another application, the resonant behavior of the crack was used to determine the depth of shallow cracks [47].

The scanning/imaging lateral resolution depends on the size of the footprint where the probe concentrates the fields (typically in the order of the diffraction limit for the near-field aperture probes). With open-ended waveguide probes, the frequency (i.e., wavelength) dictates the waveguide aperture dimensions [101], which in turn dictates the lateral imaging resolution [53], [58], [77]. It is established that the near-field lateral resolution for aperture probes is half the largest aperture dimension [53], [65]. This is primarily due to the fact that, in the vicinity of the aperture, the fields are focused within a footprint which is comparable to the aperture size. Table I shows the comparison between the spatial resolution (lateral) obtained using some of the reported near-field aperture probes [77]. To enhance the sensitivity and/or resolution of the near-field waveguide probes, tapering the aperture and loading it dielectrics/resonators were successfully demonstrated as well [56], [57], [58], [59], [60], [61], [62], [63].

As emphasized earlier, the probe's lateral resolution affects the shape (width) of the measured crack indication. The response of the near-field probe to a crack is often reported as a line scan (spatially indexed measurement parameter as the probe traverses across the crack). This is demonstrated here through experimental comparison between probes with various aperture sizes/shapes and at various lift-offs. Fig. 9(a) shows the comparison of the line scans (crack indication) represented in terms of the normalized change in $|S_{11}|$ measured at the
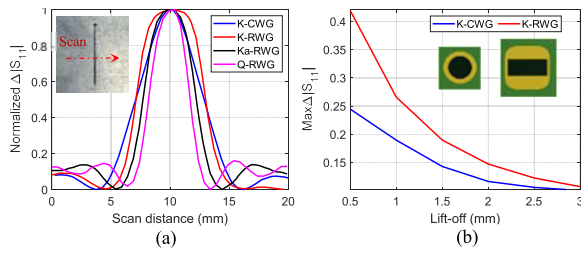
Fig. 9. (a) Normalized response (line scan) obtained using various aperture probes. (b) Sensitivity as a function of lift-off at 24 GHz.

input of various aperture probes[5] when scanned over a notch of width 0.25 mm and a length of 40 mm at a lift-off of 1 mm. The notch is made through a ∼12-mm-thick aluminum slab. The considered probes are K-band CWG with a 6.25-mm aperture diameter operating with the dominant TE_{11} mode [53] and RWG operating at 24 GHz, as well as Ka-band and Q-band (33–50 GHz) RWGs operating at 35 GHz. In the K- and Ka-bands, the frequency which yielded the maximum sensitivity for this particular notch in each band was selected (i.e., 24 and 35 GHz, respectively). The through notch used herein is longer than the aperture size of all the considered probes. The notch was scanned with the apertures arranged such that the electric field vector is orthogonal to the crack length. It is clear that the width of the response becomes smaller when higher frequency bands are used with the RWG probes (higher band implies smaller aperture [see Fig. 8(a)].

Due to its smaller aperture, the loaded K-band CWG provides higher lateral resolution than the K-band rectangular aperture [53]. Therefore, the crack indication obtained using this probe is narrower. However, it is less sensitive compared to the K-band RWG working at the same frequency. This is illustrated in Fig. 9(b) which reports the maximum change in the measured $|S_{11}|$ as a function of lift-off for both probes. This loss of sensitivity is attributed to the mode mismatch between the circular TE_{11} mode and the notch TE_{m0p} modes illustrated earlier in Figs. 2(b) and 3. On the other hand, the RWG with the TE_{10} mode excites the TE_{m0p} modes within the crack more efficiently.

It is remarked here that the range of the (linear) magnitude of the reflection coefficient is 0–1. Therefore, a change of 0.1 in $|S_{11}|$ is considered significant. It is 10% of full scale and large compared to the uncertainty in measuring $|S_{11}|$ using well-designed reflectometers.

The shape of the waveguide aperture sets up the boundary conditions for the EM field distributions (i.e., modes). However, in a noncontact application, the field distribution within the footprint determines the crack indication once scanned by the probe at a certain lift-off. Besides the loss of sensitivity due to increasing the lift-off, the field spatial distribution (and consequently, the crack indication) also changes. To illustrate this, Fig. 10 shows the line scans of the same notch described above with rectangular and circular apertures, reported in terms of the change in the magnitude and phase of the reflection coefficient. It is apparent in Fig. 10 that the general shape of the crack indication changes as the lift-off increases
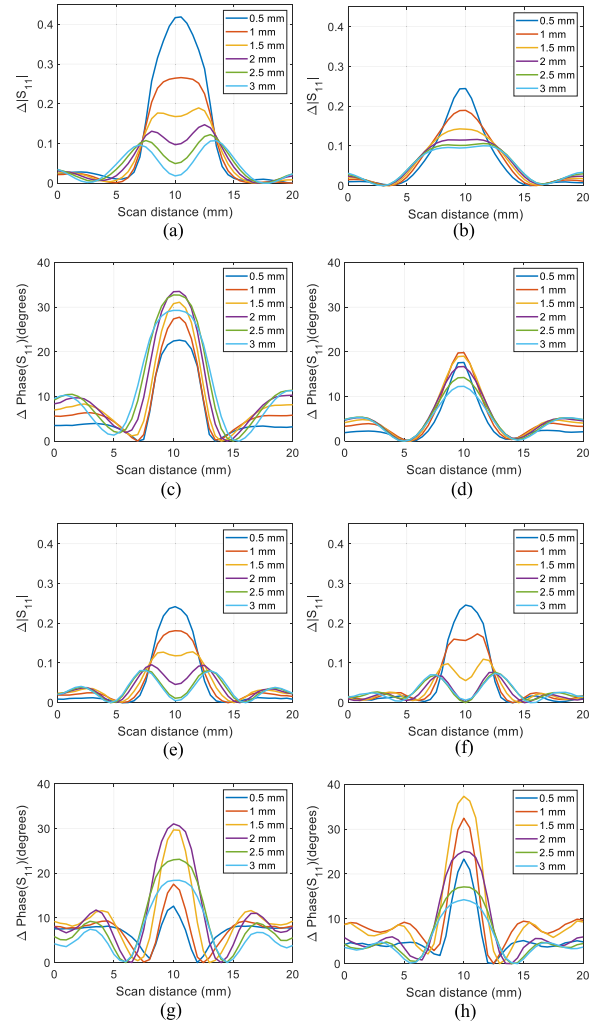
Fig. 10. Line scan of a 0.25-mm-wide notch at various lift-off using near-field aperture probes: (a) K-band rectangular (mag.); (b) K-band circular (mag.); (c) K-band rectangular (phase); (d) K-band circular (phase); (e) Ka-band rectangular (mag.); (f) Q-band rectangular (mag.); (g) Ka-band rectangular (phase); and (h) Q-band rectangular (phase).

(especially in the magnitude response). It is also observed that, while the sensitivity of $|S_{11}|$ to the notch monotonically decreases as the lift-off increases for all the probes, this is not necessarily the case for the change in the phase of S_{11}.

These experiments also showed that using a higher frequency RWG band, such as Ka- and Q-band in this case, improved the spatial resolution slightly but did not offer sensitivity improvement compared to the K-band probe. Among all aperture probes considered in this example, the K-band RWG probe provided the highest sensitivity in terms of the magnitude response. While the K-band probe showed the highest sensitivity for this particular notch geometry, this observation cannot be extrapolated to other cases in general.

As discussed earlier, the crack behaves like a cavity. Therefore, the optimum frequency of operation depends on a number of factors including the crack length and depth [41]. These determine if a resonant mode within the crack is excited efficiently with the devised near-field probe. It is further emphasized here that a real crack in practice never resembles a notch, and therefore, the optimum frequency found for a notch may not be optimum for a real crack. For instance, previous
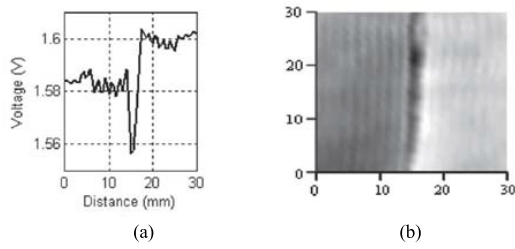
(a) (b)

Fig. 11. (a) 1-D profile and (b) image of a covered fatigue crack under 0.2-mm-thick tape obtained at 90 GHz with 1.7-mm lift-off [46] (© 2009 IEEE).

(a) (b)

Fig. 12. (a) PCB slit samples. (b) Line scans of the slits at various lift-off distances using a K-band circular aperture probe (24 GHz).

investigations on real stress-induced cracks have shown that operating at 24 GHz in the K-band is less sensitive than operating at 33 GHz in the Ka-band [42].

Open-ended waveguides when operated in their dominant mode are linearly polarized, and hence, they cannot be used to screen for cracks of arbitrary orientations [33]. On the other hand, coaxial probes are better suited for this due to the radial electric field components near the coaxial opening [28], [29], [32]. Compared to open-ended waveguides, coaxial probes provide better lateral resolution and can be operated over a wider frequency range [12]. However, their sensitivity drops significantly as the lift-off increases. Similar to the CWG, they suffer from the mode mismatch issue (TEM to TE_{m0p} in the crack).

Dual-polarized circular apertures can be used to detect cracks of arbitrary orientation as demonstrated recently in [54]. CWGs with modes incorporating radial or circumferential polarization (e.g., TM_{01}) can also be potentially used to detect cracks of any orientation [104]. However, such a near-field probe is expected to yield lower sensitivity than an RWG (due to the mode mismatch with the crack TE modes).

The RWG remains the most sensitive near-field probe reported thus far. It has been demonstrated to detect and characterize real cracks under challenging application conditions. For example, Fig. 11 shows a 1-D profile and image of a fatigue crack covered under 0.2-mm-thick tape obtained using a W-band RWG operating at 90 GHz at 1.7-mm lift-off [46]. The considered fatigue crack is similar to the one reported in Fig. 5 with an opening of 0–5 μm.

Crack characterization (e.g., sizing and/or tip location determination) using aperture and coaxial probes based on numerical and analytical modeling of the interaction between the crack and near-field probes has been considered extensively [28], [29], [30], [33], [34], [38], [39], [43], [45], [48]. The sizing methods rely on mapping the change in the measurement parameter to the crack parameters. As mentioned earlier, in the resonance region (crack length is greater than half-wavelength), the wave propagates into the crack, and the reflection measurement becomes very sensitive to the depth [17]. However, in this region, the mapping between the crack depth and reflection level is not necessarily one-to-one [17] (i.e., the crack depth cannot be determined unambiguously from the measurement). However, correlating the resonant frequency (as opposed to the reflection coefficient magnitude/phase) to the crack depth in this region may yield a one-to-one mapping. For instance, shallow crack depth determination based on its quarter-wavelength resonant response was investigated using the near-field method and reported in [47].
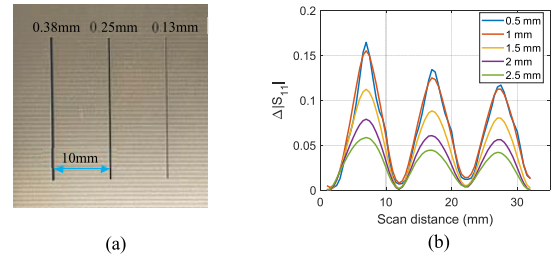
The mapping between the reflection coefficient and the width of the crack at a given crack depth can be unique as demonstrated experimentally in [42]. For instance, Fig. 12(a) shows long slits of various widths made in 1-oz copper cladding (thickness of ~35 μm) of a printed circuit board (PCB) and Fig. 12(b) shows a typical line scan of these slits at various lift-offs. In this case, the change in the magnitude of the reflection coefficient, $|S_{11}|$, is mapped (one-to-one) to the slit width at any of the considered lift-off.

C. Resonator Methods

Open-resonators employ inefficient EM radiating elements designed to concentrate the field in the proximity of the main radiating structure to increase the sensitivity and resolution [67], [68], [69], [70], [71], [72], [73], [74], [75], [76], [77], [78], [79], [80], [81], [82]. These methods were successfully demonstrated to detect 8- and 2-μm-wide fatigue cracks in steel in 1973 [67] and 1975 [68].

The basic principle of crack detection using open resonator probes is discussed in [68]. The existence of the crack perturbs the fields around the resonator, initiating a shift in its resonant frequency and/or its quality factor. Most of the resonator methods utilize the perturbation of the evanescent fields. They share with the near-field approaches; the basic fact that the presence of the crack changes the input impedance of the probe or the transfer impedance between two ports of the same resonator structure. Besides using the shift of the resonant frequency and/or change in the quality factor, the crack could also be detected with high sensitivity from the change in the reflection/transmission at the resonant frequency. Crack sizing using resonator methods relies on mapping the shift of the resonant frequency and/or the transmission/reflection level at resonance to the crack parameters. For instance, the measured level of the detected signal at resonance was used to accurately estimate crack depths ranging from ~25 to 150 μm using X-band system operating at 10 GHz [68].

The earliest microstrip-based resonator probe developed for crack detection is shown in Fig. 13(a) [68]. In this design, the aperture underneath the microstrip line is the main radiating/sensing element which interacts with the crack. The sensitivity of these techniques for crack detection is commonly quantified by the realized shift in resonant frequency (Δf_r), change in the response at the resonant frequency, or change in the quality factor for a given crack width. Fig. 13(b) illustrates an example of the transmission response between the resonator ports when the probe is scanned over crack.

The lateral resolution of the resonator probes depends on the size of the footprint where the resonator concentrates the
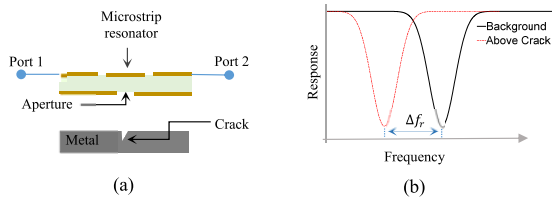
Fig. 13. (a) Microstrip resonator probe published in 1975 [68]. (b) Example resonator probe response.

fields [68]. Similar to the near-field probes, the footprint size depends on the dimension of the radiating element [68], [71]. Since these methods rely on the interaction between the evanescent fields and the crack, their lateral imaging resolution is much better than the diffraction limit. To achieve such super-resolution, the size of the main radiating element within the resonator should be much smaller than the wavelength [68]. For example, the diameter of the aperture in the resonant probe reported in [68] is around 0.3 mm which is equivalent to $\lambda/100$ at 10 GHz. A spatial resolution of about 0.15 mm ($\lambda/200$), or half the aperture size, was reported with this probe [68]. However, the resonator probe design is subject to an inherit tradeoff between sensitivity and resolution [71]. The sensitivity is high only within a very short range of lift-offs. This range is generally smaller than the size of the main radiating element in the resonator (e.g., the aperture in [68]). At a given lift-off, larger radiating elements within the resonator tend to yield lower spatial resolution and higher sensitivity [71].

The basic planar probe concept first described in [68] was subsequently utilized to realize sensitivity-enhanced probes. Inspired by the microstrip resonator probe reported in [69] and [70], the dual-behavior resonator probe was demonstrated to detect notches of width 0.2 mm at 13 GHz [71]. Similar probes with other resonator types such as complementary split-ring resonators (CSRRs) operating around 5 GHz [72] and its enhanced version which operates around 8 GHz [74] were also reported to detect notches with a width of 0.1 and 0.2 mm, respectively. It is remarked here that, unlike the probe reported in [72], [73], and [74], the probe proposed in [71] demonstrated the capability of detecting notches in two orthogonal orientations at air lift-off with actual detection through scanning. However, the efficacy of these probes to detect real cracks is yet to be demonstrated. The recently proposed resonator probes were not thoroughly compared to the classical designs (see [68]) or the near-field probes toward assessing the potential improvements in sensitivity or spatial resolution. Furthermore, the frequency of operation was mostly selected based on constraints related to the realization/design of the resonator without considering the crack frequency response.

The majority of resonators reported after the classical design introduced in [68] are applied either in contact with the surface under examination [74] or applied with a very small lift-off to yield the required sensitivity. The sensitivity of the reported noncontact resonator probes drops significantly as the lift-off increases beyond a few tens to a few hundreds of micrometers [71]. Such a small lift-off is hard to maintain or control in practice due to several reasons including the possibility of surface curvature/roughness and/or the existence
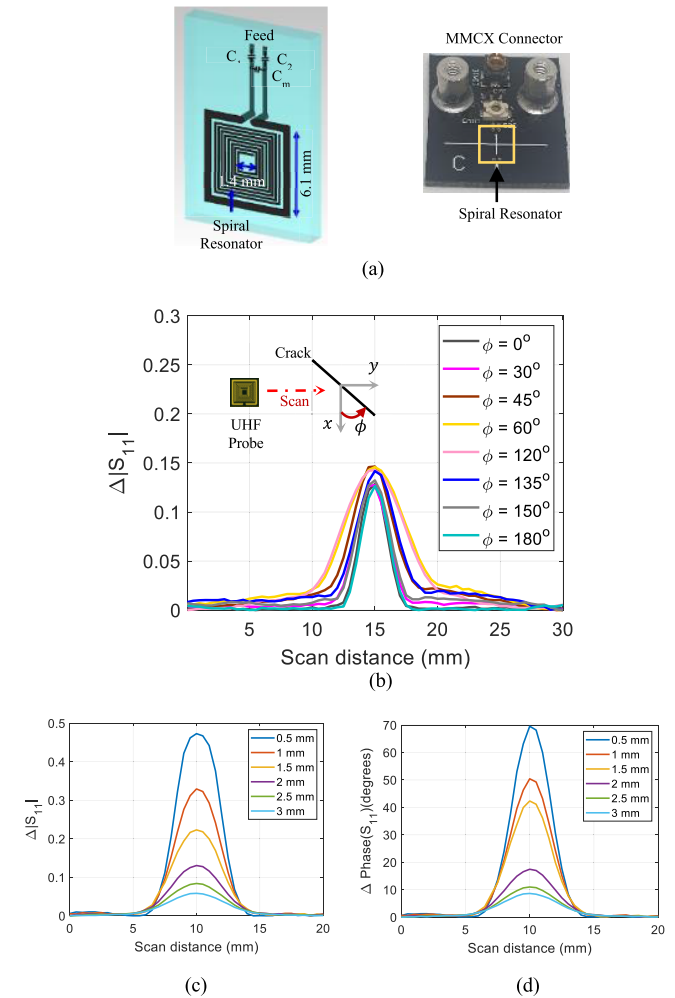

Fig. 14. (a) Model and photograph of the planar SR-loaded loop. (b) Reflection response to arbitrarily oriented crack [77] (© 2020 IEEE). (c) Magnitude line scan as a function of lift-off. (d) Phase line scan as a function of lift-off.

of dirt/dust/corrosion on the surface. Due to the limitation on lift-off, the sensitivity of these resonators to depth variations reduces after a certain crack depth.

To improve upon the abovementioned limitations, the planar resonant probe shown in Fig. 14(a) was introduced recently [76], [77], [78], [80], [81]. This one-port probe is based on a small loop loaded with a spiral resonator (SR) and can be operated at multiple resonant frequencies (modes) below 1 GHz (e.g., 500–800 MHz), in the ultrahigh frequency (UHF) band [76], [77], [81]. Therefore, it operates at a lower frequency than all other resonant probes developed for crack detection thus far.

Unlike the previously developed resonant probes, this probe was demonstrated to detect arbitrarily oriented exposed and covered cracks under insulation at lift-offs up to a few millimeters [77], [81]. The UHF probe intrinsically yields a crack indication which is fairly independent of the relative orientation between the crack and probe [77]. For example, Fig. 14(b) illustrates the response of the UHF probe as the crack's orientation varies. Fig. 14(c) and (d) shows the magnitude and phase line scans of a 0.25-mm-wide and 40-mm-long notch (much shorter than the wavelength) for various lift-offs. Furthermore, this UHF probe was successfully used to image cracks in corroded samples and performed favorably in terms
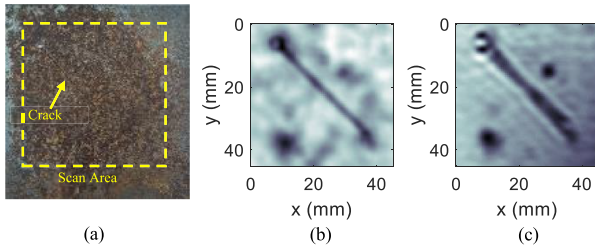
Fig. 15.   (a) Photograph of corroded metal sample with crack. (b) Image obtained using the UHF probe at a 1-mm lift-off when the sample is covered under 0.1 mm of tape. (c) Image obtained using Ka-band RWG probe for the same sample and conditions [81] (© 2022 IEEE).
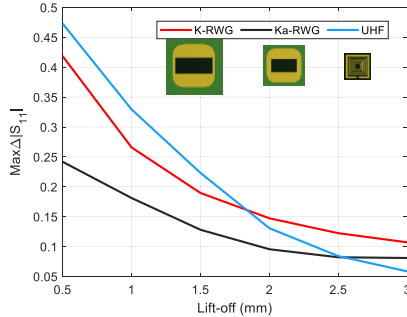

Fig. 16.   Sensitivity of the UHF probe compared to K- and Ka-band rectangular aperture probes.
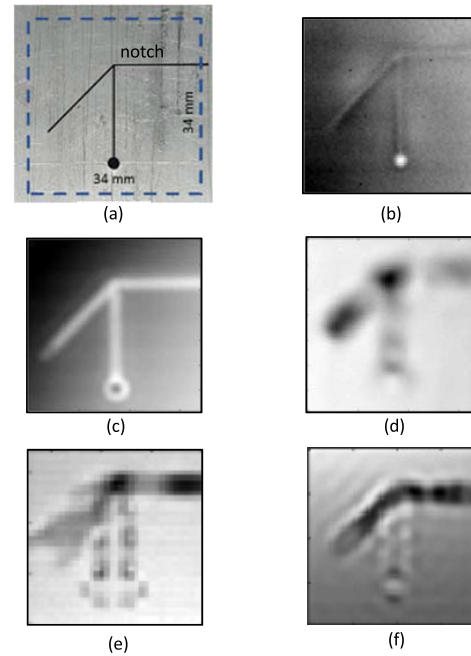

Fig. 17.   (a) Crack sample and images obtained at 1-mm lift-off using: (b) coaxial probe at 10 GHz; (c) UHF probe at 780 MHz; (d) dual-polarized circular aperture probe at 24 GHz [77] (© 2020 IEEE); (e) K-band RWG aperture at 24 GHz [54] (© 2019 IEEE); and (f) Ka-band RWG aperture at 36 GHz.
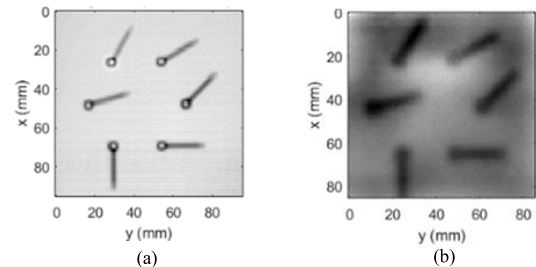

Fig. 18.   Magnitude images obtained using the UHF probe for the crack sample shown in Fig. 6(b) at 1 mm of lift-off: (a) uncovered at 804 MHz and (b) covered under a 3-mm-thick layer of rubber at 528 MHz.

of its sensitivity and resolution relative to near-field probes working at much higher frequencies. An example of this recent application is shown in Fig. 15(a)–(c) [81].

By comparing the results reported in Fig. 14(c) and (d) with those shown in Fig. 10, the UHF probe demonstrates better overall sensitivity for this particular notch, relative to the aperture probes especially at small lift-offs. Compared to the rectangular Ka-band aperture probe, the UHF probe provides considerable sensitivity improvement up to lift-offs of 2 mm, as demonstrated in Fig. 16. It provides a sensitivity improvement of 5% compared to the K-band rectangular aperture probe up to 1 mm of lift-off (see Fig. 16) for this particular notch.

The realized improvement in sensitivity irrespective of the crack orientation is also manifested in the images obtained for a 0.25-mm-wide notch samples like the one reported in Fig. 17. The attained improvement in crack detection using the UHF probe can be readily inferred from the relative quality of the obtained images using this probe compared to those acquired using the coaxial, K-band dual-polarized circular, K-band rectangular aperture [54], [77], and Ka-band rectangular aperture probes. The images reported in Fig. 17 were all acquired at 1 mm of lift-off. Besides detecting the crack with any orientation, the UHF probe has been shown to provide a multifold increase in the image signal-to-noise ratio (SNR) compared to the near-field probes [77].

The UHF probe was also recently demonstrated to detect narrow notches covered under various dielectric materials [81]. It was used to image the notch sample reported in Fig. 6(b) while the cracks were exposed (no cover) and while covered under a 3-mm-thick layer of rubber. Fig. 18 shows the magnitude images obtained at a 1-mm lift-off for both cases.

The UHF probe is very sensitive to discontinuities in the conductor while being relatively insensitive to environmental disturbances such as surface irregularities. To demonstrate this, the probe was used to image a narrow cut with an average width of 45 μm made through a thin copper foil. The photograph in Fig. 19(a) shows the foil sample with some surface variations. The image obtained using the UHF probe with 1 mm of lift-off shows a very strong indication of the cut compared to the background variations due to the surface irregularities.

The current UHF probe has dimensions of 6.1 × 6.1 mm. It is limited in lateral resolution to 3 mm [77]. Its lateral imaging resolution can be improved in the future by miniaturizing the resonator. Developing crack characterization methods and optimizing the set of modes which can be excited with the given geometry for detection/characterization would further improve the utility of this probe.

V. Emerging Methods

A. Active Microwave Thermography

AMT is an integrated NDT&E technique based on microwave and thermographic inspection methods [86], [87], [88], [89], [90]. In AMT, incident EM energy is utilized for
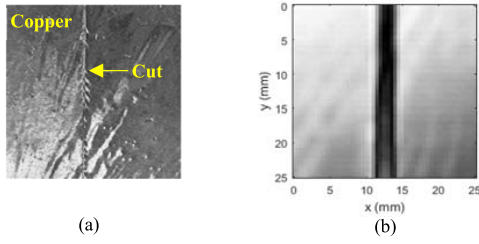
Fig. 19. (a) Photograph of copper foil with a 45-μm cut and (b) magnitude image obtained using the UHF probe at 1 mm of lift-off.
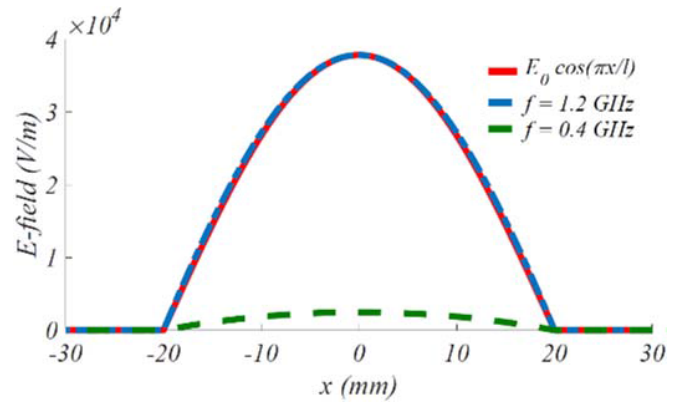

Fig. 20. Simulated E-field as a function of position along the crack length with $l = 40$ mm for below (0.4 GHz) and above cutoff (1.2 GHz) [86] (© 2019 IEEE).
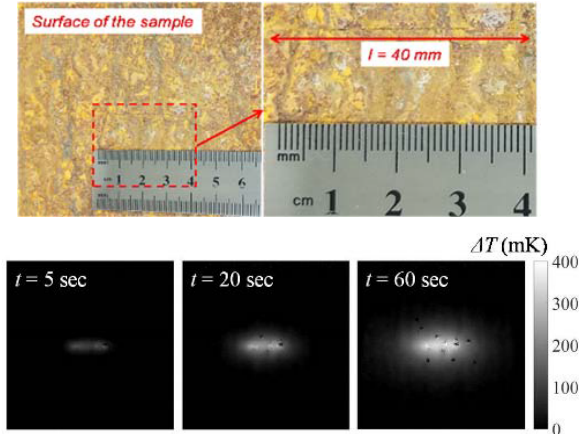

Fig. 21. Photograph of sample with surface crack (top) and measured TC (bottom) after 5, 20, and 60 s of microwave illumination [86] (© 2019 IEEE).

the thermal excitation, and the subsequent surface thermal profile of the structure/material under test is measured with an infrared (thermal) camera. Utilizing an EM-based excitation facilitates the technique to be tailored to the inspection need through choice of frequency, EM signal polarization, and power level (among other parameters). During an AMT inspection and depending on the material under the test, two heating mechanisms may occur, referred to as dielectric heating and induction heating. Dielectric heating results from absorption of microwave energy in lossy dielectric materials and serves as the primary thermal excitation for most AMT applications. On the other hand, induction heating occurs due to current induced on the surface of conductive materials and manifests through ohmic losses. The induced surface current can also serve as a secondary source of radiated (scattered) EM energy which may in turn be absorbed by nearby dielectrics.

AMT has been successfully applied to civil infrastructure and aerospace inspections needs including inspection of cement-based structures [87], [88], detection of moisture ingress [89], and inspection of microwave absorbing topcoats [90]. AMT has been successfully applied to the inspection of corroded metal structures for the presence of cracks [86]. As discussed in [86], AMT is capable of detecting filled cracks in metal structures due the lossy dielectric contained within the crack (in this case, corrosion) and the fact that the crack behaves as a very short waveguide. This implies an inherent frequency restriction, as there must be electric field coupled into the crack in order for the crack filling to absorb the EM energy and manifest as an increase in temperature within a surface thermal image.

To illustrate this, a crack with length, l, of 40 mm (broad dimension) and width, w, of 0.3 mm is simulated considering 2.4-GHz plane wave incidence with 50-W average power. The crack is assumed to be filled with corrosion (modeled as a relative permittivity of 10). For this case, the cutoff frequency for TE$_{10}$ (dominant) mode generated within the crack is ∼1.2 GHz, meaning that dielectric heating may occur for frequencies greater than 1.2 GHz, as this is the frequency at which the incident electric field (E-field) will couple into the filled-crack waveguide (i.e., resonant crack). To highlight this effect, the E-field distribution in the crack for frequencies of 0.4 (below cutoff) and 1.2 GHz (slightly above cutoff) is illustrated in Fig. 20. Also included is the TE$_{10}$ mode distribution, $E_0 \cos(\pi x/l)$, where x is the position along the length of the crack and E_0 is the amplitude of the E-field at $x = 0$. As seen, the E-field for $f = 1.2$ GHz agrees well with that of the TE$_{10}$ mode distribution, whereas for $f = 0.4$ GHz, the magnitude of the E-field is much lower (due to evanescent

waves), thus illustrating the waveguide-like behavior of the crack.

Measurements were also conducted on a representative sample similar to the geometry considered in simulation. The sample has a machined crack with $l \cong 40$ mm and $w \cong 0.15$ mm. On the surface of the sample, there is a thin corrosion layer (around 0.1 mm thick) that covers the crack. An operating frequency of 2.4 GHz as chosen as it is above the cutoff frequency for a crack of this length and also falls within the unlicensed frequency band allocated for industrial, scientific and medical (ISM) applications. A photograph of the crack sample is shown in Fig. 21.

The crack sample was irradiated using a horn antenna at a 150-mm lift-off. Prior to microwave illumination, the sample was at thermal equilibrium with a temperature of T_a. After microwave illumination, the temperature increase, $\Delta T(t)$, can be expressed as the difference between the absolute temperature, $T(t)$, at time t, and the ambient temperature of the structure, T_a, as $\Delta T(t) = T(t) - T_a$. From this and to facilitate quantitative study of the temperature variation on the surface of sample, the thermal contrast, TC, is considered. The TC is defined as the difference between the temperature increase at the crack location, $\Delta T_D(t)$, and that of a crack-free (sound) area, $\Delta T_S(t)$, as TC $= \Delta T_D(t) - \Delta T_S(t)$. In general, the TC must be at minimum equal to the sensitivity of the thermal camera for successful detection after t second of microwave illumination (i.e., heating time). The TC for the

TABLE II
OVERVIEW OF THE MICROWAVE CRACK DETECTION METHODS

Ref.	Year	Crack/Notch Width (mm)	Lift-off (mm)	Freq. (GHz)	Cover Thickness (mm) /Material	Approach	Probe/Antenna	Preferred Orientation
[16]	1970	0.05	5	30.5	N.A	Far-field[#]	Mode conversion w circ. horn	No
[68]	1975	0.002[$]	< 0.35	10	N.A.	Resonant	Aperture w/ microstrip resonator	NR
[17]	1979	0.25	NR	100	N.A.	Far-Field	Mode conversion w lens-focused horn	No
[26]	1994	0.034	0	12	N.A.	Near-Field	Open-ended Coaxial	No
[33]	1994	0.84	0	24	N.A.	Near-Field	Rectangular aperture	Yes
[37]	1996	0.3	0	24	N.A.	Near-Field	Rectangular aperture	Yes
[39]	1997	0.51	1	24	1/Wrapping paper	Near-Field	Rectangular aperture	Yes
[42]	2000	~0.0 − 0.05[$]	0	24&33	N.A.	Near-Field	Rectangular aperture	Yes
[71]	2008	0.2[*]	<0.25	~8/13	N.A.	Resonant	Dual-behavior filter	No
[46]	2009	~0-0.005[$]	1.7	90	0.2/tape	Near-Field	Rectangular aperture	Yes
[72]	2012	0.1 & 0.2[*]	0	~5	0.07/Teflon	Resonant	CSRR under microstrip	Yes
[31]	2013	0.26	0	14-16	0.1,0.2/PVC	Near-Field	Open-ended Coaxial	No
[32]	2014	0.152	0	10	N.A.	Near-Field	Open-ended Coaxial	No
[60]	2014	0.025-0.1[&]	0.6	16.6	N.A.	Near-Field	SRR-Loaded rectangular aperture	NR
[74]	2017	0.2[*]	0	~8	0.07/Teflon	Resonant	Slot patterns under microstrip	Yes
[19]	2017	0.15 (x[$])	9	26.5-40	1/Corrosion	Far-field-SAR	Rectangular aperture	Yes
[62]	2018	1-3[*]	0.5	12.5	N.A.	Near-Field	Loaded rectangular aperture	NR
[54]	2019	0.25	1	24	N.A.	Near-Field	Dual-polarized circular aperture	No
[61]	2019	1[*]	0	16	N.A.	Near-Field	Loaded rectangular aperture	NR
[22]	2020	0.5 (x[$])	100	26.5-40	N.A.	Far-field-SAR	Dual circ. polarized square aperture	No
[21]	2020	0.25-0.875	30	26.5-40	N.A.	Far-field-SAR	Rectangular aperture	Yes
[77]	2020	0.25	1	~0.8	N.A.	Resonant	Loop loaded with spiral resonator	No
[75]	2020	1	0	1.5-3.5	N.A.	Resonant	Array of CSRR	No
[23]	2020	>1	~10	22-26	N.A.	Far-field-SAR	Linearly polarized circular aperture	Yes
[24]	2021	0.25	10	24	4-12.7/Rubber/Teflon	Far-field-SAR	Dual-polarized circular aperture	No
[25]	2021	2	>1000	12.4-18	N.A.	Far-field-SAR	Linearly polarized horn	No
[85]	2021	1	1	1	N.A.	Resonant	Forced Resonance Cavity	Yes
[81]	2022	0.25	1	0.5/0.8	0.1-3/tape/paper/rubber	Resonant	Loop loaded with spiral resonator	No
[63]	2022	0.07-0.75	1	26	N.A.	Near-Field	Iris Loaded circular aperture	Yes

[$]Real crack; (x[$]): Also tested on real crack; [&]Spliced metal boards; [*] Cut model; [#]Tested in the Fresnel-zone, N.A.: not applicable (exposed). NR: Not reported

sample after 5, 20, and 60 s of microwave illumination is also shown in Fig. 21. As seen, the crack is evident in all three measurement results.

B. RFID Methods

These methods are applied by placing an RFID tag on the surface under examination and monitoring the backscattered signal remotely using a reader. These methods relay on the perturbation of the backscattered signal from an RFID tag due to the crack altering the current around the tag (i.e., its antenna). The methods assume that the location of the crack is known or it develops in the vicinity (i.e., underneath) of the scatterer/tag. They are considered contact methods despite the fact that the detection is performed remotely. Therefore, these methods are proposed for monitoring (not detecting/screening) the growth of an identified crack. The basic sensing mechanism is actually a near-field one (i.e., changing one or more characteristics of a scatterer tightly coupled to the crack). However, the detection mechanism is far field as the backscattered field or a quantity derived from it such as the radar cross section is used [91], [92], [93], [94], [95], [96], [97], [98], [99].

VI. DISCUSSION

Some of the microwave and millimeter-wave crack detection methods which are cited in this article are listed chronologically in Table II. The crack detection techniques were applied over a wide frequency range (from 0.5 to 100 GHz) using a variety of methods and probes. Some of the reported methods thus far have demonstrated detection of exposed and covered hairline cracks. Also, detecting cracks of arbitrary orientations hidden under thick covers and/or large lift-off has been demonstrated recently using some of the methods listed in Table II.

Table II lists the crack/notch width which was considered in the measurements/experimental validation. Except for the ones identified with a symbol in the width column, most of the methods were tested on the notch model similar to the one shown in Fig. 1(c). As shown in Table II, a few of the methods were actually demonstrated on real tight cracks and many considered relatively wide notches. Also, some of these methods were demonstrated only in contact while others have been applied with an air lift-off.

The methods which require a specific orientation between the crack and the probe cannot detect cracks of arbitrary orientation. Such methods generally have a lower chance of discovering the crack without scanning the surface under examination at multiple angles. Therefore, the methods which do not have a preferred orientation are deemed practically more appealing, especially when the crack is hidden under cover/paint/corrosion.

The far-field methods possess many attractive features for crack detection. These methods enable detection of exposed and covered cracks at large lift-offs without being sensitive to variation in this important parameter. However, the application of the imaging far-field methods requires scanning over large apertures. In the future, imaging systems which enable one-shot imaging similar to the ones reported

in [105] and [106] could be deployed specifically for crack detection.

The near-field methods applied particularly with RWGs have shown great efficacy for crack detection and characterization. Such methods enabled the detection of real cracks in flat surfaces and in challenging locations (e.g., close to fasteners). The near-field methods can be applied with lift-offs up to a few millimeters. However, their response is sensitive to lift-off variation. This challenge has been addressed by the introduction of the lift-off compensation techniques [64], [65]. The application of RWGs toward detecting arbitrarily oriented cracks is limited. Other near-field probes such as the dual-polarized CWGs were proposed and devised to detect arbitrarily oriented cracks. However, they exhibit loss in sensitivity due to the mode mismatch. In the future, the dual-polarized square waveguide similar to the one reported in [22] could be used as well. Similar to the imaging far-field methods, the near-field methods require scanning. To speed up the crack screening process, arrays of probes similar to the one proposed in [50] could be used.

The application of the resonator probes, with the exception of the UHF probe [76], [77], [78], [80], [81], is limited in sensitivity to contact (with known crack location) or very near-contact applications. This limits their utility for crack detection in a real environment. Real crack detection with the majority of the recently proposed resonator probes has not been reported. On the other hand, the UHF probe has exceptional performance for detecting exposed and covered cracks of arbitrary orientation at lift-offs extending to a few millimeters. When compared to the near-field probes on the same set of samples, it consistently provided better detection performance. Similar to the other scanned methods, the application of the UHF probe for crack detection requires mechanical scanning. In the future, using a near-field array of UHF probes similar to the one reported in [77] could be used to enable faster screening.

The emerging method based on microwave thermography offers key practical benefits. This method could be applied at large lift-off. Compared to all other methods, microwave thermography allows screening for cracks over large area of examination without the need to scan the antenna. The detection capability is mainly limited by the transmitted power and the thermal sensitivity of the detector. It has been demonstrated on resonant cracks filled with lossy material. The envelope of operation for this promising method will be further established in future investigations.

Most of the methods which were in fact qualified in detecting real cracks can be realized using fairly similar systems. However, operating at lower frequencies and/or within a narrow band implies lower system complexity and cost. With the exception of microwave thermography, the required power level is low. The far-field methods generally require more power to render detection at larger lift-off compared to the near-field and resonator methods. The methods realized with planar/printed probes tend to be less expensive compared to the ones realized using waveguides.

VII. Conclusion

Detecting cracks in metals is critical for structural health monitoring and integrity assessment. Microwave and millimeter-wave NDT&E techniques have demonstrated great potential to detect and characterize hidden and exposed cracks of arbitrary orientations in a noncontact fashion and at large lift-off. A myriad of probes and methods were developed and optimized for various inspection applications. Each of these methods/probes has its own merits and disadvantages.

It is demonstrated in the overviewed literature that microwave and millimeter-wave NDT&E can provide viable inspection solutions. The future research should be focused on addressing the challenges which hinder the acceptance of these methods as standard NDT&E techniques. Some of the identified research and development directions are outlined below.

The representativeness of the defects used in the qualification tests is of paramount importance for the assessment of any NDT&E tool. This entails focusing the efforts on detecting and characterizing cracks emulated to give crack indications similar to the ones encountered in practical inspection scenarios. The acceptance of the developed methods will be dependent upon the successful application of the method to real cracks.

With the exception of a few studies, analyzing and subsequently optimizing the detection performance under realistic environmental disturbances and uncertainty sources remain largely absent from the literature. Statistical analysis on the detection performance will significantly assist in demonstrating the reliability of the proposed techniques.

Direct comparisons with standard NDT&E modalities which are well-established/accepted in the industry are needed to demonstrate the relative performance, merits, and limitations. Ideally, these comparisons should consider benchmarking against the state-of-the-art NDT&E technologies.

Development of application procedures, standards, guidelines, and calibration methods will widen the utility of the techniques. Alignment of key terms such as resolution and sensitivity with the available industry standards is viewed as catalyst for proper technology positioning within the NDT&E domain.

References

[1] A. Mann, "Forensic engineering: Cracks in steel structures," *Proc. Inst. Civil Engineers*, vol. 164, no. FE1, pp. 15–23, Feb. 2011.

[2] J. Wåle and P. Ekström, "Crack characterisation for in-service inspection planning," SAQ Kontroll AB, Stockholm, Sweden, SKI Projekt 14.4-940389, SAQ/FoU-Rapport 95/70, 1995.

[3] J. Wåle, "Crack characterisation for in-service inspection planning: An update," SKI, Stockholm, Sweden, SKI Report 2006:24, 2006.

[4] T. Marazani, D. M. Madyira, and E. T. Akinlabi, "Repair of cracks in metals: A review," *Proc. Manuf.*, vol. 8, pp. 673–679, 2017.

[5] Y. Yao, S.-T.-E. Tung, and B. Glisic, "Crack detection and characterization techniques—An overview," *Structural Control Health Monitor.*, vol. 21, no. 12, pp. 1387–1413, Dec. 2014.

[6] R. M. Meyer, "Review of NDE methods for detection and monitoring of atmospheric SCC in welded canisters for the storage of used nuclear fuel," Pacific Northwest Nat. Lab. (PNNL), Richland, WA, USA, Tech. Rep. PNNL-22158, 2013.

[7] P. Shull, *Nondestructive Evaluation: Theory, Techniques, and Applications*, Cleveland, OH, USA: CRC Press, 2002.

[8] A. J. Bahr, "Microwave eddy-current techniques for quantitative non-destructive evaluation," in *Eddy-Current Characterization of Materials and Structures*, vol. 722. West Conshohocken, PA, USA: ASTM STP, 1981, pp. 311–331.

[9] A. J. Bahr, "Microwave nondestructive testing methods," in *Nondestructive Testing Monographs and Tracts; Gordon and Breach*. New York, NY, USA: Science, 1982.

[10] R. Zoughi, *Microwave Non-Destructive Testing and Evaluation*. The Netherlands: Kluwer Academic, 2000.

[11] S. Kharkovsky and R. Zoughi, "Microwave and millimeter wave nondestructive testing and evaluation—Overview and recent advances," *IEEE Instrum. Meas. Mag.*, vol. 10, no. 2, pp. 26–38, Apr. 2007.

[12] R. Zoughi and S. Kharkovsky, "Microwave and millimeter wave sensors for crack detection," *Fatigue Fract. Eng. Mater. Struct.*, vol. 31, no. 8, pp. 695–713, 2008.

[13] M. U. Memon and S. Lim, "Review of electromagnetic-based crack sensors for metallic materials (recent research and future perspectives)," *Metals*, vol. 6, no. 8, p. 172, Aug. 2016.

[14] K. Brinker, M. Dvorsky, M. T. Al Qaseer, and R. Zoughi, "Review of advances in microwave and millimetre-wave NDT&E: Principles and applications," *Phil. Trans. Roy. Soc. A, Math., Phys. Eng. Sci.*, vol. 378, no. 2182, Sep. 2020, Art. no. 20190585.

[15] L. Feinstein and R. J. Hrby, "Surface crack detection by microwave methods," in *Proc. 6th Symp. Nondestruct. Eval. Aerosp. Weapons Syst. Compon. Mater.*, San Antonio, TX, USA, 1967, pp. 1–2.

[16] R. J. Hruby and L. Feinstein, "A novel nondestructive, noncontacting method of measuring the depth of thin slits and cracks in metals," *Rev. Sci. Instrum.*, vol. 41, no. 5, pp. 679–683, May 1970.

[17] A. J. Bahr, "Using electromagnetic scattering to estimate the depth of a rectangular slot," *IEEE Trans. Antennas Propag.*, vol. AP-27, no. 6, pp. 738–746, Nov. 1979.

[18] M. T. Ghasr, K. P. Ying, and R. Zoughi, "SAR imaging for inspection of metallic surfaces at millimeter wave frequencies," in *Proc. IEEE Int. Instrum. Meas. Technol. Conf. (IMTC)*, May 2014, pp. 1202–1206.

[19] J. R. Gallion and R. Zoughi, "Millimeter-wave imaging of surface-breaking cracks in steel with severe surface corrosion," *IEEE Trans. Instrum. Meas.*, vol. 66, no. 10, pp. 2789–2791, Oct. 2017.

[20] A. Zhuravlev, V. Razevig, S. Ivashov, A. Skrebkov, and V. Alekseev, "On the use of microwave holography to detect surface defects of rails and measure the rail profile," *Sensors*, vol. 19, no. 6, p. 1376, Mar. 2019.

[21] M. Dvorsky, M. T. Al Qaseer, and R. Zoughi, "Crack sizing using dual-polarized microwave SAR imaging," in *Proc. IEEE Int. Instrum. Meas. Technol. Conf. (IMTC)*, Dubrovnik, Croatia, May 2020, pp. 1–6.

[22] M. Dvorsky, M. T. A. Qaseer, and R. Zoughi, "Detection and orientation estimation of short cracks using circularly polarized microwave SAR imaging," *IEEE Trans. Instrum. Meas.*, vol. 69, no. 9, pp. 7252–7263, Sep. 2020.

[23] M. Chizh, A. Zhuravlev, V. Razevig, and S. Ivashov, "Non-destructive testing of the rails rolling surface and joints with synthetic aperture radar," in *Proc. 21st Int. Radar Symp. (IRS)*, Oct. 2020, pp. 112–116.

[24] M. A. Abou-Khousa and M. S. U. Rahman, "Covered cracks detection using dual-polarization synthetic aperture radar imaging," *IEEE Trans. Instrum. Meas.*, vol. 70, pp. 1–4, 2021.

[25] T. Watanabe and H. Yamada, "Orientation estimation of surface cracks in metals based on intensity maximization of polarimetric circular synthetic aperture radar images," *IEEE Trans. Instrum. Meas.*, vol. 70, pp. 1–14, 2021.

[26] N. Qaddoumi, S. Ganchev, and R. Zoughi, "A novel microwave fatigue crack detection technique using an open-ended coaxial line," in *Proc. Conf. Precis. Electromagn. Meas. Dig.*, 1994, pp. 59–60.

[27] M. Saka, Y. Ju, D. Luo, and H. Abe, "A method for nondestructive evaluation of crack depth on metal surface by microwaves," in *Proc. 25th Int. Conf. Infr. Millim. Waves*, 2000, pp. 423–424.

[28] Y. Wang and R. Zoughi, "Interaction of surface cracks in metals with open-ended coaxial probes at microwave frequencies," *Mater. Eval.*, vol. 2000, 58, pp. 1228–1234.

[29] N. Wang and R. Zoughi, "Moment method solution for modeling the interaction of open ended coaxial probes and surface cracks in metals," *Mater. Eval.*, vol. 60, no. 10, pp. 1253–1258, 2002.

[30] H. Maftooli, H. R. Karami, S. H. H. Sadeghi, and R. Moini, "Output signal prediction of an open-ended coaxial probe when scanning arbitrary-shape surface cracks in metals," *IEEE Trans. Instrum. Meas.*, vol. 61, no. 9, pp. 2384–2391, Sep. 2012.

[31] S.-H. Yang, K.-B. Kim, and J.-S. Kang, "Detection of surface crack in film-coated metals using an open-ended coaxial line sensor and dual microwave frequencies," *NDT E Int.*, vol. 54, pp. 91–95, Mar. 2013.

[32] K. M. Donnell, A. McClanahan, and R. Zoughi, "On the crack characteristic signal from an open-ended coaxial probe," *IEEE Trans. Instrum. Meas.*, vol. 63, no. 7, pp. 1877–1879, Jul. 2014.

[33] C.-Y. Yeh and R. Zoughi, "A novel microwave method for detection of long surface cracks in metals," *IEEE Trans. Instrum. Meas.*, vol. 43, no. 5, pp. 719–725, Oct. 1994.

[34] C. Yeh and R. Zoughi, "Microwave detection of finite surface cracks in metals using rectangular waveguides," *Res. Nondestruct. Eval.*, vol. 6, no. 1, pp. 35–55, 1995.

[35] C. Yeh and E. R. Ranu Zoughi, "A novel microwave method for surface crack detection using higher order waveguide modes," *Mater. Eval.*, vol. 52, no. 6, pp. 676–681. Jun. 1994.

[36] C. Y. Yeh and R. Zoughi, "Sizing technique for slots and surface cracks in metals," *Mater. Eval.*, vol. 53, no. 4, pp. 496–501, 1995.

[37] C. Huber and R. Zoughi, "Detecting stress and fatigue cracks," *IEEE Potentials*, vol. 15, no. 4, pp. 20–24, Oct. 1996.

[38] C. Huber, H. Abiri, S. I. Ganchev, and R. Zoughi, "Analysis of the 'crack characteristic signal' using a generalized scattering matrix representation," *IEEE Trans. Microw. Theory Techn.*, vol. 45, no. 4, pp. 477–484, Apr. 1997.

[39] C. Huber, H. Abiri, S. I. Ganchev, and R. Zoughi, "Modeling of surface hairline-crack detection in metals under coatings using an open-ended rectangular waveguide," *IEEE Trans. Microw. Theory Techn.*, vol. 45, no. 11, pp. 2049–2057, Nov. 1997.

[40] C. Huber et al., "Remote detection of surface cracks/slots using open-ended rectangular waveguide sensors: An experimental investigation," *Nondestruct. Test. Eval.*, vol. 13, no. 4, pp. 37–227, 1997.

[41] R. Z. S. Ganchev and C. Huber, "Microwave measurement-parameter optimization for detection of surface breaking hairline cracks in metals," *Nondestruct. Test. Eval.*, vol. 14, no. 5, pp. 323–327, 1998.

[42] N. Qaddoumi, E. Ranu, J. D. McColskey, R. Mirshahi, and R. Zoughi, "Microwave detection of stress-induced fatigue cracks in steel and potential for crack opening determination," *Res. Nondestruct. Eval.*, vol. 12, no. 1, pp. 87–103, 2000.

[43] F. Mazlumi, S. H. H. Sadeghi, and R. Moini, "Analysis technique for interaction of rectangular open-ended waveguides with surface cracks of arbitrary shape in metals," *NDT E Int.*, vol. 36, pp. 331–338, Jul. 2003.

[44] F. Mazlumi, S. H. H. Sadeghi, and R. Moini, "Using open-ended rectangular waveguide probe for detection and sizing of fatigue cracks in metals," *Electron. Lett.*, vol. 41, no. 6, pp. 334–335, Mar. 2005.

[45] F. Mazlumi, S. H. H. Sadeghi, and R. Moini, "Interaction of rectangular open-ended waveguides with surface tilted long cracks in metals," *IEEE Trans. Instrum. Meas.*, vol. 55, no. 6, pp. 2191–2197, Dec. 2006.

[46] S. Kharkovsky, M. T. Ghasr, and R. Zoughi, "Near-field millimeter-wave imaging of exposed and covered fatigue cracks," *IEEE Trans. Instrum. Meas.*, vol. 58, no. 7, pp. 2367–2370, Jul. 2009.

[47] A. McClanahan, S. Kharkovsky, A. R. Maxon, R. Zoughi, and D. D. Palmer, "Depth evaluation of shallow surface cracks in metals using rectangular waveguides at millimeter-wave frequencies," *IEEE Trans. Instrum. Meas.*, vol. 59, no. 6, pp. 1693–1704, Jun. 2010.

[48] A. M. Yadegari, R. Moini, S. H. H. Sadeghi, and F. Mazlumi, "Output signal prediction of an open-ended rectangular waveguide probe when scanning cracks at a non-zero lift-off," *NDT E Int.*, vol. 43, no. 1, pp. 1–7, Jan. 2010.

[49] F. Mazlumi, N. Gharanfeli, S. H. H. Sadeghi, and R. Moini, "An open-ended substrate integrated waveguide probe for detection and sizing of surface cracks in metals," *NDT E Int.*, vol. 53, pp. 36–38, Jan. 2013.

[50] I. Ahanian, S. H. H. Sadeghi, and R. Moini, "An array waveguide probe for detection, location and sizing of surface cracks in metals," *NDT E Int.*, vol. 70, pp. 38–40, Mar. 2015.

[51] A. Yassin, M. S. U. Rahman, and M. A. Abou-Khousa, "Imaging of near-surface defects using microwaves and ultrasonic phased array techniques," *J. Nondestruct. Eval.*, vol. 37, no. 4, pp. 1–8, Dec. 2018.

[52] Y. Yu, Y. Li, H. Qin, and X. Cheng, "Microwave measurement and imaging for multiple corrosion cracks in planar metals," *Mater. Design*, vol. 196, Nov. 2020, Art. no. 109151.

[53] M. R. Ramzi, M. Abou-Khousa, and I. Prayudi, "Near-field microwave imaging using open-ended circular waveguide probes," *IEEE Sensors J.*, vol. 17, no. 8, pp. 2359–2366, Apr. 2017.

[54] M. A. Abou-Khousa, M. S. Rahman, and X. Xingyu, "Dual-polarized microwave imaging probe," *IEEE Sensors J.*, vol. 19, no. 5, pp. 1767–1776, Mar. 2019.

[55] H. H. Park, Y. H. Cho, and H. J. Eom, "Surface crack detection using flanged parallel-plate waveguide," *Electron. Lett.*, vol. 37, no. 25, pp. 1526–1527, Dec. 2001.

[56] M. T. Ghasr, S. Kharkovsky, R. Zoughi, and R. Austin, "Comparison of near-field millimeter-wave probes for detecting corrosion precursor pitting under paint," *IEEE Trans. Instrum. Meas.*, vol. 54, no. 4, pp. 1497–1504, Aug. 2005.

[57] S. Kharkovsky, A. McClanahan, R. Zoughi, and D. D. Palmer, "Microwave dielectric-loaded rectangular waveguide resonator for depth evaluation of shallow flaws in metals," *IEEE Trans. Instrum. Meas.*, vol. 60, no. 12, pp. 3923–3930, Dec. 2011.

[58] N. N. Qaddoumi, M. Abou-Khousa, and W. M. Saleh, "Near-field microwave imaging utilizing tapered rectangular waveguides," *IEEE Trans. Instrum. Meas.*, vol. 55, no. 5, pp. 1752–1756, Oct. 2006.

[59] T. Yun and S. Lim, "High-Q and miniaturized complementary split ring resonator-loaded substrate integrated waveguide microwave sensor for crack detection in metallic materials," *Sens. Actuators A, Phys.*, vol. 214, pp. 25–30, Aug. 2014.

[60] B. Hu, Z. Ren, M. S. Boybay, and O. M. Ramahi, "Waveguide probe loaded with split-ring resonators for crack detection in metallic surfaces," *IEEE Trans. Microw. Theory Techn.*, vol. 62, no. 4, pp. 871–878, Apr. 2014.

[61] Q. Wang et al., "High-sensitivity dielectric resonator-based waveguide sensor for crack detection on metallic surfaces," *IEEE Sensors J.*, vol. 19, no. 14, pp. 5470–5474, Jul. 2019.

[62] X. Yang et al., "Array waveguide probe loaded with split-ring resonators for sizing the cracks in metal surface," *IEEE Microw. Wireless Compon. Lett.*, vol. 28, no. 2, pp. 171–173, Feb. 2018.

[63] M. S. U. Rahman, O. S. Hassan, and M. A. Abou-Khousa, "Crack detection and corrosion mapping using loaded-aperture microwave probe," *IEEE Open J. Instrum. Meas.*, vol. 1, pp. 1–11, 2022.

[64] M. T. Ghasr, B. J. Carroll, S. Kharkovsky, R. Zoughi, and R. Austin, "Millimeter-wave differential probe for nondestructive detection of corrosion precursor pitting," *IEEE Trans. Instrum. Meas.*, vol. 55, no. 5, pp. 1620–1627, Oct. 2006.

[65] M. A. Abou-Khousa, S. Kharkovsky, and R. Zoughi, "Novel near-field millimeter-wave differential probe using a loaded modulated aperture," *IEEE Trans. Instrum. Meas.*, vol. 58, no. 5, pp. 1273–1282, May 2009.

[66] Y. Gao et al., "Millimeter wave differential probe system for surface crack detection in painted aircraft fuselage," in *Proc. IEEE Int. Instrum. Meas. Technol. Conf. (IMTC)*, May 2019, pp. 1–6.

[67] E. A. Ash and A. Husain, "Surface examination using a superresolution scanning microwave microscope," in *Proc. 3rd Eur. Microw. Conf.*, Oct. 1973, pp. 1–4.

[68] A. Husain and E. A. Ash, "Microwave scanning microscopy for non-destructive testing," in *Proc. 5th Eur. Microw. Conf.*, Hamburg, Germany, Sep. 1975, pp. 213–217.

[69] M. Tabib-Azar, N. S. Shoemaker, and S. Harris, "Non-destructive characterization of materials by evanescent microwaves," *Meas. Sci. Technol.*, vol. 4, no. 5, pp. 583–590, May 1993.

[70] R. Wang, F. Li, and M. Tabib-Azar, "Calibration methods of a 2 GHz evanescent microwave magnetic probe for noncontact and nondestructive metal characterization for corrosion, defects, conductivity, and thickness nonuniformities," *Rev. Sci. Instrum.*, vol. 76, no. 5, May 2005, Art. no. 054701.

[71] J. Kerouedan et al., "Detection of micro-cracks on metal surfaces using near-field microwave dual-behavior resonator filters," *Meas. Sci. Technol.*, vol. 19, pp. 1–10, Aug. 2008.

[72] A. M. Albishi, M. S. Boybay, and O. M. Ramahi, "Complementary split ring resonator for crack detection in metallic surfaces," *IEEE Microw. Wireless Compon. Lett.*, vol. 22, no. 6, pp. 330–332, Jun. 2012.

[73] A. Albishi and O. Ramahi, "Detection of surface and subsurface cracks in metallic and non-metallic materials using a complementary split-ring resonator," *Sensors*, vol. 14, pp. 70–19354, 2014.

[74] A. M. Albishi and O. M. Ramahi, "Microwaves-based high sensitivity sensors for crack detection in metallic materials," *IEEE Trans. Microw. Theory Techn.*, vol. 65, no. 5, pp. 1864–1872, May 2017.

[75] A. Salim, A. H. Naqvi, A. D. Pham, and S. Lim, "Complementary split-ring resonator (CSRR)-loaded sensor array to detect multiple cracks: Shapes, sizes, and positions on metallic surface," *IEEE Access*, vol. 8, pp. 151804–151816, 2020.

[76] M. A. Abou-Khousa, K. T. M. Shafi, and X. Xingyu, "High-resolution UHF near-field imaging probe," *IEEE Trans. Instrum. Meas.*, vol. 67, no. 10, pp. 2353–2362, Oct. 2018.

[77] A. Haryono, K. Aljaberi, M. S. U. Rahman, and M. A. Abou-Khousa, "High resolution and polarization independent microwave near-field imaging using planar resonator probes," *IEEE Access*, vol. 8, pp. 191421–191432, 2020.

[78] M. A. Abou-Khousa and A. Haryono, "Array of planar resonator probes for rapid near-field microwave imaging," *IEEE Trans. Instrum. Meas.*, vol. 69, no. 6, pp. 3838–3846, Jun. 2020.

[79] Z. Xie, Y. Li, L. Sun, W. Wu, R. Cao, and X. Tao, "A simple high-resolution near-field probe for microwave non-destructive test and imaging," *Sensors*, vol. 20, no. 9, p. 2670, May 2020.

[80] M. S. Rahman, A. A. Mustapha, and M. A. Abou-Khousa, "Detection and sizing of surface cracks in metals using UHF probe," in *Proc. IEEE Intern. Conf. Imaging Syst. Techn. (IST)*, Aug. 2021, pp. 1–5.

[81] M. S. Ur Rahman, A. A. Mustapha, and M. A. Abou-Khousa, "Detection of cracks under cover and corrosion using UHF probe," in *Proc. IEEE Int. Instrum. Meas. Technol. Conf. (IMTC)*, May 2022, pp. 1–5.

[82] Z. Chen, X. Q. Lin, Y. H. Yan, F. Xiao, M. T. Khan, and S. Zhang, "Noncontact group-delay-based sensor for metal deformation and crack detection," *IEEE Trans. Ind. Electron.*, vol. 68, no. 8, pp. 7613–7619, Aug. 2021.

[83] K.-C. Kim, J.-Y. Kwon, and N.-W. Kang, "A novel forced-resonance microwave method to detect surface cracks in metal," *IEICE Electron. Exp.*, vol. 13, no. 17, 2016, Art. no. 20160715.

[84] K.-C. Kim, J.-W. Kim, J.-Y. Kwon, and N.-W. Kang, "Characteristics of a cutoff cavity probe applicable to crack detection using the forced resonance microwave method," *J. Electromagn. Eng. Sci.*, vol. 20, no. 4, pp. 285–292, Oct. 2020.

[85] K.-C. Kim, J.-W. Kim, J.-Y. Kwon, and N.-W. Kang, "Non-contact crack detection in metals using a cutoff-cavity probe," *J. Electromagn. Eng. Sci.*, vol. 21, no. 3, pp. 167–176, Jul. 2021.

[86] A. Foudazi, A. Mirala, and M. T. Ghasr, "Active microwave thermography for nondestructive evaluation of surface cracks in metal structures," *IEEE Trans. Instrum. Meas.*, vol. 68, no. 2, pp. 576–585, Feb. 2019.

[87] A. Foudazi, C. A. Edwards, M. T. Ghasr, and K. M. Donnell, "Active microwave thermography for defect detection of CFRP-strengthened cement-based materials," *IEEE Trans. Instrum. Meas.*, vol. 65, no. 11, pp. 2612–2620, Nov. 2016.

[88] A. Foudazi, I. Mehdipour, K. M. Donnell, and K. H. Khayat, "Evaluation of steel fiber distribution in cement-based mortars using active microwave thermography," *Mater. Struct.*, vol. 49, no. 12, pp. 5051–5065, Dec. 2016.

[89] A. Mirala, A. Foudazi, M. T. A. Qaseer, and K. M. Donnell, "Active microwave thermography to detect and locate water ingress," *IEEE Trans. Instrum. Meas.*, vol. 69, no. 12, pp. 9774–9783, Dec. 2020.

[90] A. Mirala, M. T. A. Qaseer, and K. M. Donnell, "Health monitoring of RAM-coated structures by active microwave thermography," *IEEE Trans. Instrum. Meas.*, vol. 70, pp. 1–11, 2021.

[91] I. Mohammad and H. Y. Huang, "An antenna sensor for crack detection and monitoring," *Adv. Struct. Eng.*, vol. 14, no. 1, pp. 47–53, Feb. 2011.

[92] A. M. J. Marindra and G. Y. Tian, "Chipless RFID sensor tag for metal crack detection and characterization," *IEEE Trans. Microw. Theory Techn.*, vol. 66, no. 5, pp. 2452–2462, May 2018.

[93] S. Caizzone and E. DiGiampaolo, "Wireless passive RFID crack width sensor for structural health monitoring," *IEEE Sensors J.*, vol. 15, no. 12, pp. 6767–6774, Dec. 2015.

[94] X. Yi, C. Cho, J. Cooper, Y. Wang, M. M. Tentzeris, and R. T. Leon, "Passive wireless antenna sensor for strain and crack sensing—Electromagnetic modeling, simulation, and testing," *Smart Mater. Struct.*, vol. 22, no. 8, Aug. 2013, Art. no. 085009.

[95] J. Zhang, G. Y. Tian, and A. B. Zhao, "Passive RFID sensor systems for crack detection & characterization," *NDT E Int.*, vol. 86, pp. 89–99, Mar. 2017.

[96] J. Zhang et al., "A configurable dielectric resonator-based passive wireless sensor for crack monitoring," *IEEE Trans. Antennas Propag.*, vol. 67, no. 8, pp. 5746–5749, Aug. 2019.

[97] S. Dey, P. Kalansuriya, and N. C. Karmakar, "Novel chipless RFID high resolution crack sensor based on SWB technology," *IEEE Sensors J.*, vol. 21, no. 3, pp. 2908–2920, Feb. 2021.

[98] M. Norouzi, N. Masoumi, and H. Jahed, "Nondestructive phase variation-based chipless sensing methodology for metal crack monitoring," *IEEE Trans. Instrum. Meas.*, vol. 70, pp. 1–11, 2021.

[99] N. Javed, M. A. Azam, and Y. Amin, "Chipless RFID multisensor for temperature sensing and crack monitoring in an IoT environment," *IEEE Sensors Lett.*, vol. 5, no. 6, pp. 1–4, Jun. 2021.

[100] C. A. Balanis, *Advanced Engineering Electromagnetics*, 2nd ed. Hoboken, NJ, USA: Wiley, 2012.

[101] D. M. Pozar, *Microwave Engineering*, 4th ed. Hoboken, NJ, USA: Wiley, 2012.

[102] *International Vocabulary of Metrology—Basic and General Concepts and Associated Terms*, document JCGM 200:2012, Joint Committee for Guides in Metrology (VIM), 3rd ed., 2012. [Online]. Available: http://www.bipm.org/en/publications/guides/vim.html

[103] C. Liu, M. T. A. Qaseer, and R. Zoughi, "Influence of antenna pattern on synthetic aperture radar resolution for NDE applications," *IEEE Trans. Instrum. Meas.*, vol. 70, pp. 1–11, 2021.

[104] M. Dvorsky, M. T. A. Qaseer, and R. Zoughi, "Polarimetric synthetic aperture radar imaging with radially polarized antennas," *IEEE Trans. Instrum. Meas.*, vol. 69, no. 2, pp. 9866–9879, Dec. 2020.

[105] M. T. Ghasr, M. A. Abou-Khousa, S. Kharkovsky, R. Zoughi, and D. Pommerenke, "Portable real-time microwave camera at 24 GHz," *IEEE Trans. Antennas Propag.*, vol. 60, no. 2, pp. 1114–1125, Feb. 2012.

[106] M. T. Ghasr, M. J. Horst, M. R. Dvorsky, and R. Zoughi, "Wideband microwave camera for real-time 3-D imaging," *IEEE Trans. Antennas Propag.*, vol. 65, no. 1, pp. 258–268, Jan. 2017.
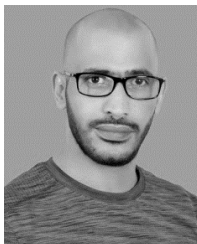
Mohamed A. Abou-Khousa (Senior Member, IEEE) received the B.S. degree (magna cum laude) from the American University of Sharjah, Sharjah, United Arab Emirates (UAE), in 2003, the M.S. degree from Concordia University, Montreal, QC, Canada, in 2004, and the Ph.D. degree from the Missouri University of Science and Technology (Missouri S&T), Rolla, MO, USA, in 2009, all in electrical engineering (EE).

From 2005 to 2009, he was a Graduate Research Assistant with the Applied Microwave Nondestructive Testing Laboratory, Missouri S&T. From 2009 to 2013, he was a Research Scientist/Engineer with the Robarts Research Institute, London, ON, Canada. He is currently an Associate Professor with the Electrical Engineering and Computer Science Department, Khalifa University of Science and Technology, Abu Dhabi, UAE. Over the course of his career, he executed various research and development projects within broad range of sectors including oil and gas, biomedical, space, and aerospace. He has coauthored many technical publications in his areas of expertise and holds several patents. His areas of expertise include RF, microwave, and millimeter-wave instrumentation, material characterization, nondestructive testing, and subsurface imaging.

Dr. Abou-Khousa was a recipient of multiple national and international awards including the IEEE Instrumentation and Measurement Society 2017 Outstanding Young Engineer Award. As a coauthor, he received the H. A. Wheeler Applications Prize Paper Award from the IEEE Antennas and Propagation Society. He currently serves as the Associate Editor-in-Chief of the IEEE TRANSACTIONS ON INSTRUMENTATION AND MEASUREMENT (TIM).

Mohammed Saif Ur Rahman received the B.S. degree in instrumentation engineering from Osmania University, Hyderabad, India, in 2011, and the M.S. degree in control and instrumentation engineering from King Fahd University, Dhahran, Saudi Arabia, in 2015.

He is currently working as a Research Associate with the Smart Sensing Systems (SSS) Group, Khalifa University of Science and Technology, Abu Dhabi, United Arab Emirates (UAE). His research interests include instrumentation, sensing systems, nondestructive testing, and microwave imaging.

Kristen M. Donnell (Senior Member, IEEE) received the B.S.E.E. degree from Colorado State University, Fort Collins, CO, USA, in 2001, and the M.S.E.E. and the Ph.D. degrees in electrical engineering from the Missouri University of Science and Technology (Missouri S&T, formerly University of Missouri–Rolla), Rolla, MO, USA, in 2003 and 2010, respectively.

She was a Systems Engineer and an Electrical Engineer with Raytheon Company, Tewksbury, MA, USA, from 2003 to 2006. She is currently an Associate Professor with the Department of Electrical and Computer Engineering, Missouri S&T, and also the Director of the Microwave Sensing (μSense) Laboratory. Her current research interests include thermography, frequency selective surfaces, materials characterization, and microwave and millimeter-wave nondestructive testing.

Dr. Donnell has been involved with the IEEE Instrumentation and Measurement Society since 2007. She currently serves as the Vice-President of the Finance Committee and the Chair of the Distinguished Lecturer Program.

Mohammad Tayeb Al Qaseer (Senior Member, IEEE) received the B.S. degree (magna cum laude) in electrical engineering from the American University of Sharjah (AUS), Sharjah, United Arab Emirates (UAE), in 2002, and the M.S. and Ph.D. degrees in electrical engineering from the Missouri University of Science and Technology (formerly University of Missouri–Rolla), Rolla, MO, USA, in 2004 and 2009, respectively.

He is currently an Associate Professor with the Electrical and Computer Engineering Department, Iowa State University, Ames, IA, USA. He has coauthored over 75 journal articles and over 100 conference proceedings and presentations. He holds 12 awarded patents in the areas of microwave and millimeter-wave imaging and nondestructive testing. His research interest is in the area of microwave and millimeter-wave instrumentation and measurement and its application for holographical measurement and 3-D synthetic aperture radar (SAR) imaging. His other interests include RF circuits, antennas, numerical electromagnetic analysis, material evaluation, and nondestructive testing.